

## **Copyright Warning & Restrictions**

The copyright law of the United States (Title 17, United States Code) governs the making of photocopies or other reproductions of copyrighted material.

Under certain conditions specified in the law, libraries and archives are authorized to furnish a photocopy or other reproduction. One of these specified conditions is that the photocopy or reproduction is not to be “used for any purpose other than private study, scholarship, or research.” If a user makes a request for, or later uses, a photocopy or reproduction for purposes in excess of “fair use” that user may be liable for copyright infringement,

This institution reserves the right to refuse to accept a copying order if, in its judgment, fulfillment of the order would involve violation of copyright law.

**Please Note: The author retains the copyright while the New Jersey Institute of Technology reserves the right to distribute this thesis or dissertation**

Printing note: If you do not wish to print this page, then select “Pages from: first page # to: last page #” on the print dialog screen

The Van Houten library has removed some of the personal information and all signatures from the approval page and biographical sketches of theses and dissertations in order to protect the identity of NJIT graduates and faculty.

## **ABSTRACT**

### **DEVELOPMENT OF A CENTRIFUGAL MICROFLUIDIC DEVICE FOR SEPARATION AND SORTING IN BIOLOGICAL FLUIDS**

**by  
Gaurav Sunil Bagwe**

A wide interest in employing micron-scale, integrated biochemical analysis systems for economical and rapid diagnosis has been the principal motivation behind this project. Low operating costs, portability and fast diagnosis times make centrifugal microfluidic devices an attractive option in patient-side diagnostics. Some essential tasks to be performed in microfluidic devices are sample-reagent transport, mixing, separation and detection. All these tasks require precise control of the RPM and spinning time. Centrifugal micro-fluidic platforms have been successfully implemented for detection of hepatitis A, tetanus, as well as for measurement of haemoglobin and hematocrit, for DNA analysis, and for assessment of cardiac disease etc. by assaying biological fluids like blood, saliva, and urine.

This thesis presents the construction, including the micro-machining and testing of a multi-channel centrifugal microfluidic device for point-of-care (POC) diagnostics. A low cost device capable of delivering controlled revolutions per minute was made by modifying a CD-ROM drive and a polymer disk was used to handle the fluids. A network of microfluidic channels and reservoirs was fabricated on the CD by using a rapid prototyping method. The reservoirs hold the biofluid sample, meter the volume of fluid accurately and also serve as a component of capillary burst valves to gate the flow of fluid. Micromachining techniques like photolithography, wet-etching have been discussed for mass production of the prototype used for this research.

Theoretical analysis of the burst frequency for passive capillary valves is reported and compared with practical results. The goal of this thesis was to develop a low cost device and demonstrate its use in the separation, and metering of plasma from blood using centrifugal microfluidics. One challenge when using blood for diagnosis is to separate the blood plasma from the rest of the blood cells. Concepts of blood centrifugation and particle displacement on a spinning disk have been employed to calculate the required RPM. Experiments were carried out on various geometries in order to achieve the maximum level of separation. The results of these experiments have been reported. It has been established that centrifugal microfluidics can be used to accurately control the flow of fluids in microchannels and this can be used for reliable low cost point-of-care diagnostics.

**DEVELOPMENT OF A CENTRIFUGAL MICROFLUIDIC DEVICE  
FOR SEPARATION AND SORTING IN BIOLOGICAL FLUIDS**

**by  
Gaurav Sunil Bagwe**

**A Thesis  
Submitted to the Faculty of  
New Jersey Institute of Technology  
in Partial Fulfillment of the Requirements for the Degree of  
Master of Science in Biomedical Engineering**

**Department of Biomedical Engineering**

**January 2011**

Blank Page

**APPROVAL PAGE**

**DEVELOPMENT OF A CENTRIFUGAL MICROFLUIDIC DEVICE  
FOR SEPARATION AND SORTING IN BIOLOGICAL FLUIDS**

**Gaurav Sunil Bagwe**

---

Dr. Max Roman, Thesis Advisor Associate Professor of Biomedical Engineering, NJIT	Date
--	------

---

Dr. William C. Van Buskirk, Committee Member Distinguished Professor and Chair of Biomedical Engineering, NJIT	Date
---	------

---

Dr. Richard A. Foulds, Committee Member Associate Professor of Biomedical Engineering, NJIT	Date
--	------

---

Dr. Hans R. Chaudhry, Committee Member Research Professor of Biomedical Engineering, NJIT	Date
--	------

## **BIOGRAPHICAL SKETCH**

**Author:** Gaurav Sunil Bagwe

**Degree:** Master of Science

**Date:** January 2011

### **Undergraduate and Graduate Education:**

- Master of Science in Biomedical Engineering,  
New Jersey Institute of Technology, Newark, NJ, 2011
- Bachelor of Science in Biomedical Engineering,  
Mumbai University, Mumbai, India, 2003

**Major:** Biomedical Engineering



This thesis is dedicated to my parents,  
Sunil Bagwe and Shubhada Bagwe, and my relatives,  
who not only cared, loved and supported me but also  
instilled a love of reading and education and taught me the value of hard work.

## **ACKNOWLEDGMENT**

I would like to thank Dr. Max Roman for his scholarly guidance for developing this thesis and his unwavering support throughout the duration of my Master's Program at NJIT. The evolution and progress of the project would have been impossible without his invaluable inputs and direction.

I would like to express my appreciation to all of the committee members for providing their valuable suggestions and inputs throughout the course of the project. A special thanks to the faculty and staff of the Department of Biomedical Engineering for teaching me advanced concepts in Biomedical Engineering and making this journey possible.

Special thanks to John Hoinowski for his time and effort in fabricating, machining parts and disks needed for prototypes. His attention to detail and constant stress on accuracy has been a major factor in obtaining repeatable results in all the experiments that were conducted during this thesis.

I am grateful to my friends, who encouraged me through countless hours of lab work. I appreciate the efforts of Varun Sivaramakrishnan and Bushra Hossain towards developing some components of the thesis and also for providing the opportunity to learn and progress together throughout my graduate school years.

Lastly, I would like to express my gratitude towards my parents for their faith, always being there for me all throughout the progress of my thesis and eventually the completion of my degree.

## TABLE OF CONTENTS

Chapter	Page
1 INTRODUCTION .....	1
1.1 Objective .....	1
1.2 Current Trends in the Point Of Care Testing Industry .....	2
1.3 Review of Different Propulsion Mechanisms.....	4
1.3.1 Electrokinetic Propulsion .....	5
1.3.2 Thermal Propulsion .....	6
1.3.3 Mechanical Propulsion .....	6
1.3.4 Centrifugal Propulsion .....	6
2 PHYSIOLOGY OF BLOOD .....	7
2.1 Components of Blood .....	7
2.1.1 Erythrocytes.....	8
2.1.2 Leukocytes .....	9
2.1.3 Thrombocytes .....	11
2.1.4 Plasma .....	11
2.2 Fluid Properties of Blood .....	12
2.3 Diagnostics Using Blood .....	13
3 EXPERIMENTAL SETUP .....	16
3.1 CD-ROM Drive Function.....	16
3.2 Device Construction .....	13
3.3 Materials .....	20

## TABLE OF CONTENTS (Continued)

Chapter	Page
3.4 Rapid Prototyping Method .....	20
3.5 Sealing Methods .....	24
3.6 Complete Experimental Setup .....	26
4 EXPERIMENTS AND PROTOCOLS .....	28
4.1 The Capillary Burst Valve .....	29
4.1.1 Derivation of the Critical Capillary Burst Condition .....	31
4.1.2 Calculation of Theoretical Values .....	33
4.2 Effects of the Coriolis Force .....	37
4.3 Mixing of Two Fluids in Microchannels .....	40
4.4 Separation of Plasma from Blood .....	44
4.4.1 Simple Geometry with Capillary Burst Valves .....	44
4.4.2 Using a Micro-Cyclone .....	45
4.4.3 Using an Accurate Metering Geometry .....	47
5 RESULTS AND DISCUSSIONS .....	50
5.1 Capillary Burst Frequency .....	50
5.2 Coriolis Switching of Flow .....	58
5.3 Mixing of Two Fluids in Microchannels .....	63
5.4 Separation of Plasma from Blood .....	64
6 CONCLUSION AND FUTURE DIRECTION .....	69
6.1 Conclusion .....	69

## TABLE OF CONTENTS (Continued)

Chapter	Page
6.2 Future Work .....	70
6.2.1 Instrumentation Upgrade .....	71
6.2.2 Microfabrication for Mass Production .....	72
6.2.3 Advanced Biochemistry for Diagnosing Different Diseases .....	73
APPENDIX A ANALYSIS OF A PARTICLE ON A SPINNING DISK .....	74
APPENDIX B DATASHEET OF THE TA8493AF .....	78
REFERENCES .....	87

## LIST OF TABLES

<b>Table</b>	<b>Page</b>
1.1 Comparison of the Different Propulsion Mechanisms .....	4
2.1 Composition of Blood .....	7
2.2 Various Types of Leukocytes and their Relative Numbers .....	10
4.1 Capillary Burst Valve Parameters for Valve at B .....	35
4.2 Capillary Burst Valve Parameters for Valve at C .....	36
5.1 Comparison of the Theoretical and Observed Values of the Critical Burst Frequencies for Water Color .....	53
5.2 Comparison of the Theoretical and Observed Values of the Critical Burst Frequencies for Anti-Coagulated Blood .....	54
5.3 Results of the Coriolis-Based Flow Switch.....	60

## LIST OF FIGURES

Figure	Page
1.1 (a) The Abaxis VetScan VS2 system, (b) rotor loaded with blood and reagent (front and back).....	3
2.1 Red blood cells under a microscope.....	9
2.2 Types of White Blood Cells.....	10
2.3 Newtonian nature of blood.....	13
3.1 TA 8493AF on the CD ROM drive PCB board.....	17
3.2 Relation between the control voltage ( $V_c$ ), reference voltage ( $V_{ref}$ ) and the duty cycle of the motor.....	18
3.3 Modified PCB of a Samsung CD-ROM Drive.....	19
3.4 Design mask used to fabricate the geometries on a CD.....	22
3.5 Specialized CD holder used in the rapid prototyping method .....	22
3.6 (a) Micro-channel with triangular cross-section, (b) Width = 290 $\mu\text{m}$ , (c) rectangular cross-section obtained by modifying the blade, (d) channel width = 250 $\mu\text{m}$ .....	23
3.7 Sealed reservoirs with pinholes as air inlets and outlets.....	25
3.8 (a) A close-up of the modified CD-ROM, (b) Complete experimental setup.....	26
4.1 Different valves used in centrifugal microfluidics.....	28
4.2 Geometry to Verify the Burst Frequency Equation.....	30
4.3 Graph of RPM versus time in seconds.....	31
4.4 Surface tension measurements of different water colors and water.....	34
4.5 Geometry used to show gating of fluid (water-color and blood) using capillary valves.....	37
4.6 Flow-switching valve on a CD.....	39

## LIST OF FIGURES (Continued)

Figure	Page
4.7 Geometries used to verify the gating of fluid using the Coriolis force.....	40
4.8 Geometry used to test the mixing of two liquids in microchannels.....	42
4.9 Schematics of (a) CD-ELISA design with 24 sets of assays, (b) a single assay, (1 waste; 2 detection; 3 first antibody; 4, 6, 8, 10 washing; 5 blocking protein; 7 antigen/sample; 9 second antibody; 11 substrate) and (c) photo of a single assay.	45
4.10 Cyclonic air purifier employed in pharmaceutical industries.....	46
4.11 Separation and metering geometry for plasma separation.....	47
4.12 Geometry of the input reservoir.....	48
5.1 Verification of capillary burst frequency carried out with water color (a) input reservoir loaded with water color, (b) water color burst into reservoir B, (c) water color burst into reservoir C.....	51
5.2 Verification of capillary burst frequency carried out with blood (a) Input reservoir loaded with blood, (b) blood burst into reservoir B, (c) blood burst into reservoir C.....	55
5.3 Experiment to find the zero leakage rpm, (a) Input reservoir filled with water color initially, (b) Leakage occurring at 630 rpm, (c) No leakage at 1050 rpm....	58
5.4 Graph of the filling ratio versus the rpm.....	61
5.5 Gating due to Coriolis force (a) Disk spinning at 680 rpm, (b) Disk spinning at 760 rpm.....	62
5.6 Mixing of two fluids in microchannels (a) after completion of spinning of the disk, (b) while the disk is still spinning.....	63
5.7 Separation of plasma from blood using a geometry with just capillary valves.....	65
5.8 Plasma separation using the micro-cyclone geometry.....	66
5.9 Separation of plasma using the metering geometry.....	66
5.10 (a) Whole blood imaged at 40X, (b) Separated plasma imaged at 40X.	67



# **LIST OF FIGURES** (Continued)

<b>Figure</b>	<b>Page</b>
A.1 Diagram of a particle on a spinning disc of radius $r$ .....	74
A.2 Free Body Diagram of a particle suspended in fluid in a reservoir.....	74
A.3 Explanation for the buoyancy force.....	75
A.4 Lateral view of a reservoir on a CD.....	76

# CHAPTER 1

## INTRODUCTION

### 1.1 Objective

The recent trends in clinical diagnosis and advances in the microfluidic technologies have created a need for translating classical, time consuming, blood-analysis procedures to compact, highly-integrated, high-throughput, high-accuracy point-of-care (POC) screening devices [3]. For a medical device to be economically acceptable it needs to provide fast and efficient diagnostic results while using minimal resources such as drugs and manual handling. The current high-throughput devices being used may be efficient but are also large, expensive machines which require large sample volumes and often lack complete sample processing abilities. These large machines require high manufacturing and maintenance costs and are usually labor intensive. Moreover, these machines are not portable and therefore require that all tests be conducted in a single location where the lab is located. Other sources for increased time-to-result for these machines is the requirement of batch processing and manual handling by qualified professionals. While these devices are advanced enough to provide highly accelerated drug discovery and automated chemical and biological tests for numerous applications, it is clear that there is a need for the development of new technologies that do not possess the significant drawbacks mentioned above. It is evident from the nature of these drawbacks that new high-throughput screening devices need to be developed by scaling down the existing systems.

Recent developments in the microfabrication and miniaturization field have given rise to micro-scale devices. Most of these devices use the flow of fluids through channels which have at least two dimensions in the micron range (less than  $10^{-6}$

meters). These systems, commonly called “lab-on-a-chip” systems have shown great promise in scaled-down, high-throughput screening used in chemical and biological diagnostics tests. Typical processes required in testing any biological fluids involve sample and reagent transportation, mixing, separation. Current diagnostic tests use the properties of fluids such as pH, electrical properties like dielectric constants etc. for diagnosis. Different microfluidic tools such as mixers, valves, pumps and flow sensors have been developed to control fluid flow, mixing, separation and reaction in these devices [1].

The main advantages afforded by microfluidic systems are low manufacturing and operation cost, low reagent and sample consumption, low time-to-result, and portability. Separate stand-alone microfluidic devices have demonstrated the ability to perform key laboratory unit operations such as sample injection, separation, mixing, reaction, metering, and detection. The microfluidic devices like LabCD which have been successfully commercialized satisfied the end-user’s stringent demands on reliability, user friendliness, and overall cost per test [1]. The objective of this thesis is to demonstrate sample mixing, separation, flow control and detection using a centrifugal microfluidic device which is low-cost, reliable and portable. This work will lay down the foundation for more comprehensive testing and analysis.

## **1.2 Current Trends in the Point-of-Care Testing Industry**

The Point-of-Care diagnostics testing industry has seen a major leap in development and commercialization of new products. One example of such commercialization is the acquisition of Gamera Biosciences microfluidics technology LabCD by a Switzerland-based company TECAN for 10 million dollars. (Source: <http://www.bioresearchonline.com>) The completion of the first stage of the Human

Genome Project is also expected to raise the demand for quick and cost-effective screening. Abbott Point-of-Care is another company which launched the i-STAT handheld blood analyzer system which provides real-time lab-quality results in minutes. The availability of fast and accurate results provides healthcare professionals the ability to make quick diagnosis and treatment decisions.



(a)



(b)

**Figure 1.1** (a) The Abaxis VetScan VS2 system, (b) rotor loaded with blood and reagent (front and back). (Source: [www.abaxis.com](http://www.abaxis.com))

The Abaxis Piccolo Express and VetScan are other commercial diagnostic products which provide complete blood analysis, in minutes from a few micro-liters (drops) of blood. Figure 1.1 shows an image of an Abaxis VetScan rotor containing the re-agents and blood sample. The Pet Care industry and veterinary medicine market is another growing industry where economical, high-throughput screening is becoming a necessity. Agriculture and nutrition also are untapped markets for such ultra high-throughput testing mechanisms.

### 1.3 Review of the Different Propulsion Mechanisms

All microfluidic systems require a mechanism to propel fluid through the micro channels at a controlled rate. The common mechanisms used to drive fluids are electrical, thermal or mechanical forces. Table 1.1 shows a comparison of the different propulsion mechanisms.

**Table 1.1** Comparison of the Different Propulsion Mechanisms ([1])

Comparison	Centrifuge	Pressure	Acoustic	Electrokinetic
Valving Solved?	Yes for liquids no for vapor	Yes for liquids and vapor	No solution shown yet for liquid or vapor	Yes for liquids no for vapor
Maturity	Products Available	Products available	Research	Products available
Propulsion force influenced by	Density and viscosity	Generic	Generic	pH, ionic strength
Power source	Rotary motor	Pump, Mechanical roller	5-40 Volts	10 kVolts
Materials	Plastics	Plastics	Piezoelectrics	Glass, Plastics
Scaling	$L^3$	$L^3$	$L^2$	$L^2$
Flow Rate	From less than 1nL/sec to greater than 100 L/sec	Very wide range (less than nL/sec to L/sec)	20 L/sec	0.001 – 1 L/sec
General Remarks	Inexpensive CD Drive, mixing is easy, most samples possible (including cells), better for diagnostics.	Standard technique. Difficult to miniaturize and multiplex.	Least mature of the four techniques. Might be too expensive. Better for smallest samples.	Mixing difficult. High voltage source is dangerous and many parameters influence propulsion, better for smallest samples (HTS)

The fundamental laws of fluid mechanics change drastically when the scale is decreased to the micron level. Electromagnetic fields, gravity, as well as surface tension and capillary forces in fluids can have considerable physical implications in these micro devices.

### **1.3.1 Electrokinetic Propulsion**

Electro-kinetic propulsion is the most popular and well-developed method in microfluidics. Fluorescence Activated Cell Sorting (FACS) is an example of electrokinetic propulsion which has been successfully carried out in microfluidic chips [2]. The common electrokinetic flow manipulation techniques are electroosmosis, electrohydrodynamics, and electrowetting [6]. The main advantage that this kind of flow affords is the ability to control the flow by simply using a series of electrodes with computer controlled voltages [28]. This technique is commonly used for electrochemical separations based on particle size and charge differences and can be successfully implemented in a plethora of materials like glass, quartz, polymers etc using microfabrication techniques. It is also easy to scale electrokinetic flow to micro levels without sacrificing the quality of results.

Electrokinetic flows also do have their share of disadvantages such as strong dependence on physical and chemical properties of the fluid like pH and ionic strength. This makes it difficult to control biological fluid flows (like blood and urine) since the varying nature of their physicochemical properties. More stringent flow control often requires higher voltages which mean lesser portability. These kinds of flows also suffer due to unwanted Faradaic reactions and air bubbles which break the continuity of fluid [6].

### **1.3.2 Thermal Propulsion**

This kind of propulsion uses locally created thermal gradients within fluid droplets for achieving flow [28]. These thermal gradients are created by embedding the surface with microheaters which can be selectively activated to create a thermal gradient within a fluid droplet. The thermal gradient causes interfacial surface tension gradient which causes the fluid droplet to flow in a manner which will lower its total associated interfacial energy. However, this technology is difficult and expensive to implement and is highly sensitive to temperature drifts.

### **1.3.3 Mechanical Propulsion**

Mechanical propulsion is an ideal method for pumping biological fluids due to its insensitivity to physicochemical properties of the fluid like pH and ionic strength. Common mechanical propulsion mechanisms include blister pouches, acoustic pumps and syringe pumps [6]. Blister pouches do not scale very well and acoustic pumps are expensive and can be implemented using only piezoelectric materials. Syringe pumps offer very good control over parameters like flow rate and volume but are not portable. Also they still require large sample size to fill up the tubes leading to the actual device.

### **1.3.4 Centrifugal Propulsion**

Centrifugal force has been found to be the most economical and easiest propulsion mechanism to propel fluids in microchannels. The device developed in this thesis also uses centrifugal force to drive the fluid through microchannels. Rotationally induced hydrostatic pressure is low cost, easy to implement and control, and insensitive to pH and ionic strength of the fluid. Moreover, it can be easily integrated with the information carrying capacity of the CD [4].

## CHAPTER 2

### PHYSIOLOGY OF BLOOD

Blood is the primary transport mechanism that delivers the required nutrients and oxygen to the different parts of the body and also removes waste such as carbon dioxide and toxins. It performs immunological functions like detection and protection from foreign materials using antibodies and white blood cells. Coagulation of blood is an important function of the body's self-repair mechanism. Other important functions of blood include regulation of body pH levels, core temperature, hydraulic functions and messenger functions carried out by hormones. Generally blood constitutes about 6-8% of the body weight in normal healthy people. [34]

#### 2.1 Components of Blood

From an engineering perspective blood is a very complex substance since it performs many different functions and its properties vary immensely depending on parameters like temperature, amount of dehydration, pH levels, pressure exerted on it, the haematocrit level of blood etc. Typical composition of blood is shown in Table 2.1.

**Table 2.1** Composition of Blood

Component	Sub-component	Percentage
<b>Erythrocytes (RBC)</b>		42 - 45%
<b>Leukocytes (WBC)</b>		0.2 - 1%
<b>Plasma</b>		55 - 60%
	Salts	1% of Plasma
	Lipids	0.6% of Plasma
	Proteins	7 - 8% of Plasma
	Glucose	0.1% of Plasma
<b>Platelets</b>		5%



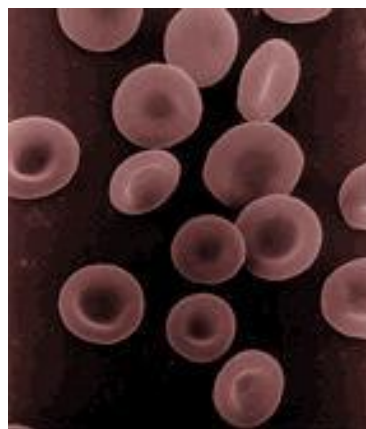
### 2.1.1 Erythrocytes

The oxygen and carbon dioxide carrying ability of blood is attributed by the red blood cells (RBC) also known as erythrocytes. One cubic millimetre of blood contains about 4-6 million erythrocytes. The word erythrocyte has been formed from a combination of the Greek words erythros for red and kytos for hollow or cell. An erythrocyte is a bi-concave disc as shown in Figure 2.1 with diameters typically varying from 8-10 micrometers. This shape gives it a large surface area to volume ratio for a single cell. The typical life span of an erythrocyte is 125 days and they are retained by the spleen at the end of their lifespan.

Red blood cells are formed in the bone marrow and contain a protein called haemoglobin which is an iron-containing metallo-protein that makes up about 97% of the dry content of each cell. Haemoglobin (also spelled as hemoglobin, abbr. Hb or Hgb) concentration is measured in most complete blood tests since it is a good indicator of anaemia. Haemoglobin readily associates and dissociates with/from oxygen and carbon dioxide which gives it a characteristic color of bright red when oxygenated and bluish-purple when de-oxygenated. Mammalian erythrocytes do not contain a nucleus which allows for more room for haemoglobin. A term called Hematocrit is defined as the proportion of blood occupied by red blood cells. It is typically three times the haemoglobin level in blood. Typical ranges of percentage hematocrit are 45-62% in males and 37-48% in females. There are similar ranges for canine and feline blood as well. These ranges can be used to diagnose Anaemia as well as Polycythemia.

Anaemia is a disease condition where the body is deficient in red blood cells whereas Polycythemia is a disease condition where the body produces excess of red blood cells. Typical symptoms of anaemia include but are not limited to weakness, or

fatigue, general malaise, poor concentration, palpitation, shortness of breath etc. Polycythemia is said to occur when the hematocrit levels rise over 55% and typical symptoms include but are not limited to headaches, vertigo, enlarged spleen and/or liver, high blood pressure and formation of blood clots in the blood stream. The centrifugal microfluidic device that will be developed aims to provide fast-screening capabilities for both anemia and Polycythemia. Figure 2.1 shows an image of some red blood cells under the microscope.



**Figure 2.1** Red blood cells under a microscope.  
(Source: <http://clinicalcenter.nih.gov>)

### 2.1.2 Leukocytes

Leukocytes, commonly known as white blood cells are the primary defence mechanism of the body. There are about 5000-7000 leukocytes in a cubic millimetre of blood. Leukocytes are classified according to their morphological appearance as Granulocytes and Agranulocytes depending on the presence of granules in the cytoplasm of these cells. Granulocytes are further classified into neutrophil, eosinophil (or acidophil) and basophil depending on their affinity towards neutral, acidic or basic stains. Agranulocytes are classified into two types: lymphocytes and monocytes. The cell structure also differs according to the type of white blood cell

and its function. The cellular structure of each type of white blood cell is shown in Figure 2.2.



**Figure 2.2** Types of White Blood Cells.

(Source: <http://www.scientificpsychic.com/mind/whitecells.html>)

It is evident from Table 2.2 that Neutrophils are the most abundant type of leukocytes. They have nuclei having two to five lobes and are the first line of defence against bacteria due to their phagocytic nature. Eosinophils are the primary defence against parasites and respond to allergies by removing fibrin formed due to inflammation. The primary function of eosinophils is the detoxification of foreign proteins [34]. The primary function of Basophils is to release histamine in the area of tissue damage. The presence of histamine causes an increase in the blood flow to that area and consequently attracts more leukocytes to the area. Each type of leukocyte in blood performs a different function and is present in different proportions as shown in Table 2.2.

**Table 2.2** Various Types of Leukocytes and their Relative Numbers

Name	Count per cubic millimeter	Size ( $\mu\text{m}$ )
<b>Neutrophil</b>	2500-7500	10-15
<b>Basophil</b>	10-100	10-12
<b>Eosinophil</b>	40-400	10-15
<b>Lymphocyte</b>	1000-3000	10-20
<b>Monocyte</b>	200-800	20-25

The primary function of Lymphocytes is to provide immunological defence against foreign invasion of the body by releasing antibody molecules which isolate antigens. They are non-phagocytic and are the highest in number after neutrophils. Monocytes are the largest leukocytes and are mobile and actively phagocytic. They contain a large central oval or indented nucleus and mature into macrophages in the body's tissues.

### **2.1.3 Thrombocytes**

Thrombocytes or platelets are granular cells without a nucleus but they do contain mitochondria. They are 1-2 micrometer cells which originate from the bone marrow, mature in the spleen for up to 36 hours and circulate in the peripheral blood for 7-10 days. The primary function of Thrombocytes is to form a mechanical plug by adhesion, secretion, aggregation and fusion in case of a vascular injury. They are vital in maintaining the haemostasis of the body in case of an injury.

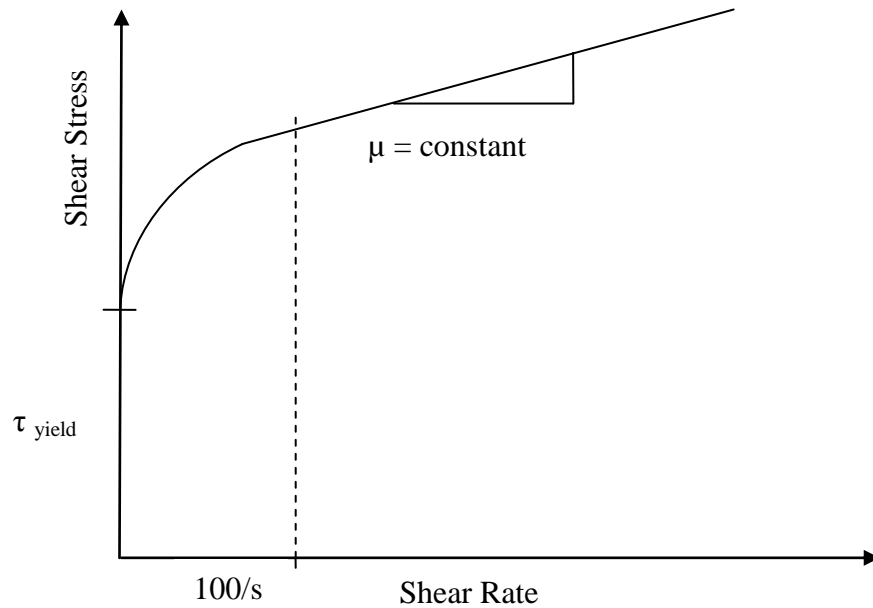
### **2.1.4 Plasma**

Plasma is the transparent, amber-colored liquid in which the cellular components of blood are suspended. One cubic milliliter of blood contains 55-60% by volume of plasma. The primary constituents of plasma are water, proteins, electrolytes, hormones and nutrients. The most important protein in plasma is the clotting protein which creates a mesh structure which the platelets fill up and seal to cover up a wound. Serum is blood plasma from which the clotting proteins have been removed. Plasma also contains other proteins which can be used to detect the presence of hyperlipidemia, cardiac disorders, etc.

## 2.2 Fluid Properties of Blood

A normal person has about 4.5 – 6.0 liters of blood in the body. Blood is slightly denser ( $1060 \text{ kg/m}^3$ ) than water ( $1000 \text{ kg/m}^3$ ) due to the increased density of red blood cells. Viscosity is an important property of a fluid. The viscosity of blood is directly related with the amount of work required to cause the blood to flow through the arteries. Typical ranges of blood viscosity are between 3 and 6 cP (centipoise) which is 0.003 and 0.006  $\text{Ns/m}^2$  [35]. Comparing this with water which has a viscosity of 7 to 10 cP at room temperature it is clear that blood is a much more viscous fluid. An extrapolation chart and typical values for whole blood viscosity have been discussed at length in [34]. Variations in viscosity, packed cell volume (PCV) or hematocrit of whole blood, etc., serve as early indicators of disease and can be used for simple screening methods.

Blood is a pre-dominantly non-Newtonian fluid, which means that its viscosity is not constant with respect to the rate of shearing strain applied on it. As discussed before blood viscosity also varies due to temperature and the haematocrit levels. However, in practical circumstances the body temperature of a human being remains constant (around  $37^\circ \text{C}$ ) and the haematocrit levels do not vary greatly with respect to time. It has been observed that if blood flows in tubes that are greater than 1 mm in diameter the viscosity of the blood remains unaffected by any changes in the rate of shearing strain (higher than  $100 \text{ s}^{-1}$ ). In such circumstances blood can be assumed to behave like a Newtonian fluid in which the shear stress and the shearing rate are related by a constant viscosity. Figure 2.3 shows a plot of the shear stress of blood versus the shearing rate at a fixed haematocrit and temperature.



**Figure 2.3** Newtonian nature of blood.

An interesting fluid property of blood is the Fahreus-Lindquist effect. It is an effect where the viscosity of a fluid changes with the diameter of the tube it is passing through. When blood flows from a reservoir into a channel (10-300 micrometers diameter), its apparent viscosity changes since the erythrocytes move towards the center of the channel, where the velocity is maximum, leaving plasma at the walls of the channel [36-37].

### 2.3 Diagnostics Using Blood

The different components of blood perform different functions within the human body. Critical information about a certain function can be gathered by simply analyzing the corresponding component of blood. The levels of proteins, hormones, lipids and glucose in blood are useful biomarkers of diseases or disorders. For example, an increased presence of RBC's may indicate the onset of Polycythemia, or excess of WBC's in the blood indicate an infection of some kind. However, to reduce the effects of other blood components in diagnosis, sorting of cells and/or plasma is

often required. The location on the body from where the blood is drawn greatly influences the chances of detecting disease markers since biomarkers may have localized presence in the circulatory systems. Miniaturization and smaller sample sizes would further degrade the chances of finding biomarkers in the collected sample. Therefore, in more complex analysis the site from where the blood sample is drawn must be specified clearly in the documentation for the test. Different types of cell-sorting mechanisms have been implemented based on the cell property used for sorting. Difference in density, sizes (diameter) have been used for mechanical sorting of cells. Electrical and magnetic properties have been explored for sorting using electro-magnetic fields. Chemical properties like antigen-antibody affinity have been successfully implemented for sorting and separating cells.

Mechanical sorting mechanisms are the most economical and therefore the most popular separation and sorting mechanisms. Screens and filters are used for sorting based on size. The use of mechanical force to accelerate sedimentation has been the most popular mechanism to sort blood cells. The centrifuge is a device which subjects blood cells to higher gravitational forces which causes the cells to sediment thus causing separation of blood. If anti-coagulated blood is collected in a test-tube and allowed to stand for a couple of hours it will ultimately sediment due to the gravitational force acting on the cells. The force due to gravity  $F$  can be given by,

$$F = mg$$

where,

$g$  = gravitational acceleration ( $9.8 \text{ m/s}^2$ )

$m$  = mass of the cell

Now if the same test-tube is placed in a centrifuge at a distance  $r$  from the center of rotation and spun at an angular velocity of  $\omega$  rad/sec the equivalent

acceleration experienced by the cell is given by  $\omega^2 r$ . Therefore the equivalent force acting on a cell is given by,

$$F = m \omega^2 r$$

This force can be increased to values much higher than the force due to gravity thereby increasing the rate of separation. Typical angular velocities for blood separation range from 3000 to 7000 rpm depending on the type of separation needed.

Despite disadvantages like lack of portability, need for large sample sizes, need for batch processing and human supervision, centrifuges still remain the primary mechanism of separating blood cells. Even after centrifugation the required component of blood needs to be carefully separated out with a micro-pipette. The device constructed in this thesis uses the principle of operation of the centrifuge but overcomes its major disadvantages.

Different schemes to separate plasma from whole blood have been implemented depending on the desired end result. Sung Yang et al. developed a microfluidic device for continuous, real-time blood plasma separation in [20] which was reported to show close to 100% plasma selectivity. L. Reigger and M. Grumann et al. [29] implemented a low-cost single-step hematocrit determination scheme on a centrifugal device which gives a direct read out of the hematocrit. However, it was found to be prone to reading errors and therefore needed to be improved. Steigert et al. developed a three-stage separation structure which used a combination of centrifugal and coriolis forces to separate plasma from blood [31].



## **CHAPTER 3**

### **EXPERIMENTAL SETUP**

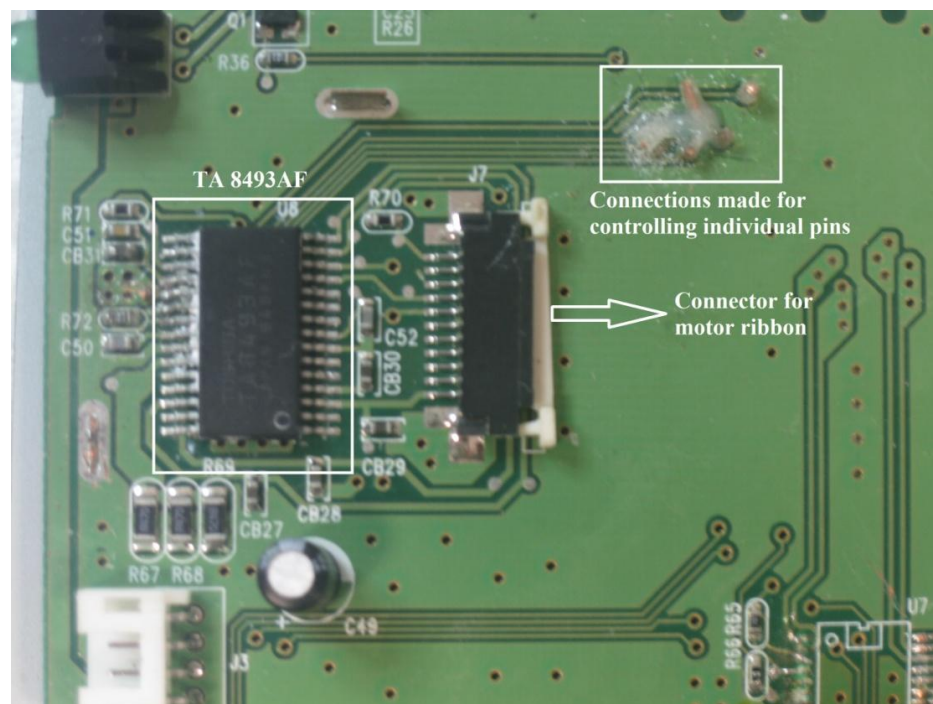
As discussed before a centrifugal microfluidic diagnostic tool requires an electronic component which can deliver controlled revolutions per minute to a polymer compact disk. A regular DC motor would have to be fitted with a custom assembly for holding the motor and the disk in place while it is rotating while keeping it centered on the axis of rotation thus keeping vibrations to a minimum. For this project, modifying an existing CD-ROM drive seemed to be the best option since it is capable of spinning disks at high rpm's without any wobble or vibrations. They already have a tray mechanism for mounting and un-mounting the disk on the motor and the ability to read and transmit data to a computer which could be used in the future.

#### **3.1 CD-ROM Drive Function**

Most CD ROM drives are rated for the maximum speed at which they can spin the discs and consequently how fast they can read and write data to/from a disc. Typically, speeds range from 10X to 52X where the X stands for the disc's nominal spin rate. A spin rate of 1X indicates that the disc is spinning at the speed of a standard audio CD (typically 500 rpm). Older CD ROM drives with speeds of 12X and below used Constant Linear Velocity (CLV). This required that the actual spin speed of the disc changes from about 210 rpm while reading from the inner tracks to about 539 rpm for the outer tracks. Modern drives however, changed to a fixed-spindle speed which is referred to as the Constant Angular Velocity (CAV) system. In this system the data transfer rate changes depending on which track the data is being transferred. (Source: <http://www.pcguide.com/ref/cd/perfRated-c.html>).

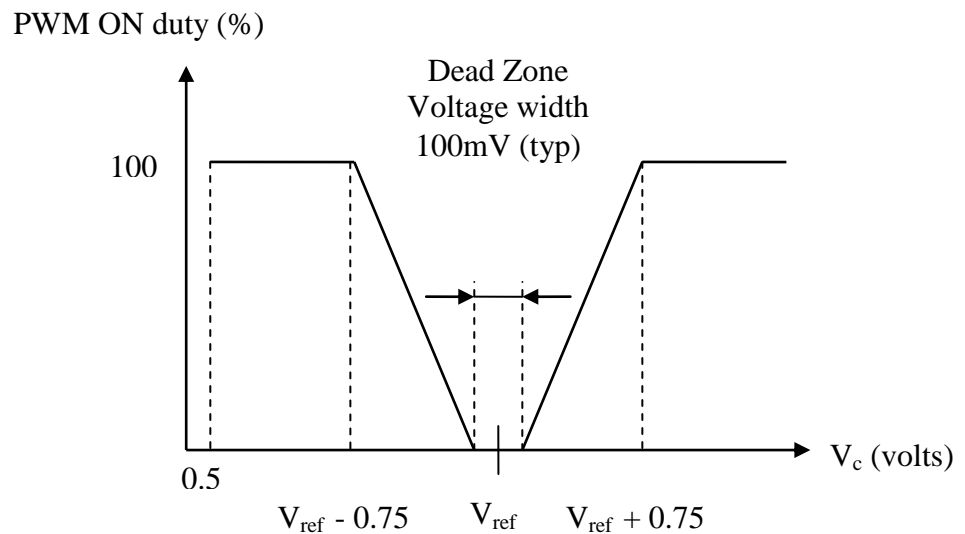
### 3.2 Device Construction

The device construction for the rpm controlled CD-ROM drive is described. The device was fabricated by modifying a Samsung CD-ROM Drive which consists of a Brushless DC Motor controlled by a 3-Phase DC Motor controller chip (Toshiba TA 8493AF). These three phase, full-wave, Brushless DC Motor Driver IC's are specialized for controlling CD-ROM drive spindle motors. The TA8493AF contains a discrete power transistor (P-ch-MOS) and uses a Direct Pulse Width Modulation (PWM) system. This means that the length of the ON time of a pulse is directly proportional to the rpm at which the disc spins. The TA 8493AF has a multi-chip structure which provides superior thermal efficiency and has a 180 degree drive system, built-in current limiter, reversing brake/short brake,  $F_g$  signal output, built-in hall-bias, and a built-in thermal shutdown circuit. Figure 3.1 shows the TA 8493AF on the PCB board of the CD ROM drive.



**Figure 3.1** TA 8493AF on the CD ROM drive PCB board.

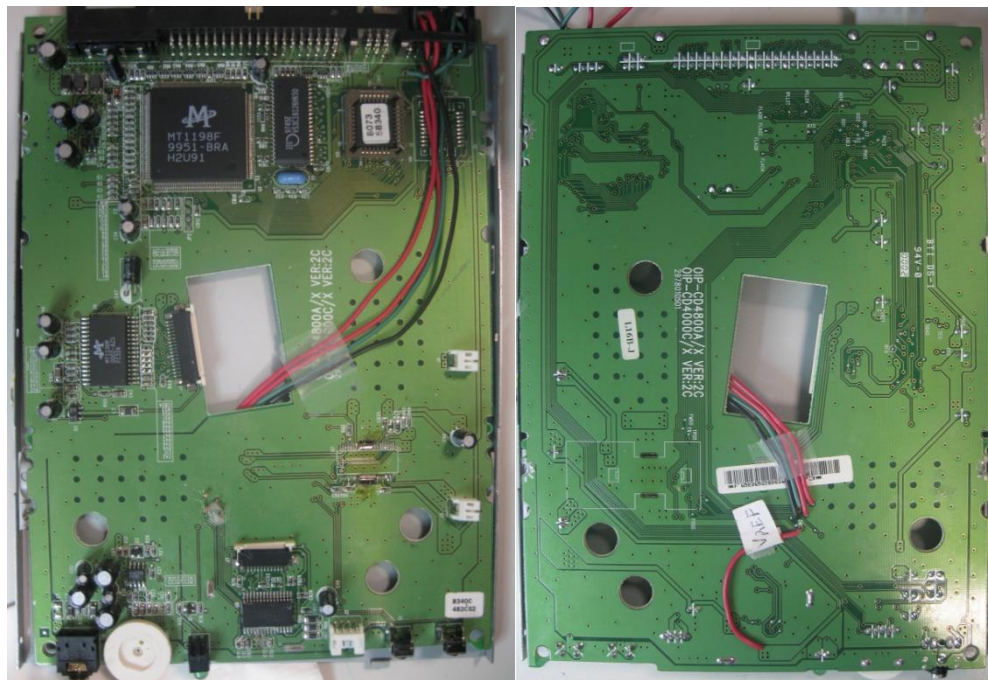
The TA 8493AF is a 40 pin IC used in the forward mode and the functions of the individual pins can be seen in the table in the datasheet attached in Appendix B. The minimum and maximum ratings are all provided in the datasheet and these ratings were carefully reviewed before energizing the chip. The chip has a reverse detection circuit which prevents the motor from rotating in a counter-clockwise direction. This is a disadvantage for the purpose of this thesis and has been explained in Section 4.2. The reversal of the spinning direction was simulated by just flipping the disk upside-down and spinning it in the default clockwise direction. The rpm output of the chip is based on the comparison of two input voltages: the control voltage ( $V_c$ ) and the reference voltage ( $V_{ref}$ ). The relation between the two input voltages and the PWM ON duty cycle is shown below.



**Figure 3.2** Relation between the control voltage ( $V_c$ ), reference voltage ( $V_{ref}$ ) and the duty cycle of the motor. (Source: Appendix B)

The input voltage ranges for both  $V_c$  and  $V_{ref}$  are 0.5 volts to 4 volts. When the difference between the two voltages exceeds 0.75 volts the PWM ON duty cycle is at 100%. If the difference between the input voltages is less than or equal to 100 millivolts the duty cycle drops to 0%. This range of voltages is known as the dead-zone

since there is no PWM output in this zone. Therefore, it is evident that to control the rpm of the CD in the forward rotation mode the control voltage  $V_c$  would have to be less than  $V_{ref}$  but not within 100 millivolts of  $V_{ref}$ . Figure 3.3 shows a modified circuit board of a Samsung CD-ROM drive. The wires have been attached to the contact points in the PCB which correspond to the pins for  $V_c$  and  $V_{ref}$ . Additionally, two more connections have been made on the PCB board. The first connection was made with the  $f_{out}$  pin (number: 10) to get a signal whose frequency is proportional to the instantaneous rpm of the disk. The second connection was made with the Run/Stop pin (number:) to enable/disable the rotation of the disk.



(a) Front

(b) Back

**Figure 3.3** Modified PCB of a Samsung CD-ROM Drive.

Braking can be used to stop the rotation of the CD by making  $V_c$  more than  $V_{ref}$  and selecting the appropriate signals for the BRK and MS (mode select) pins. Using the braking feature would have speeded up the whole process of waiting for the disc to come to a standstill before it can be ejected from the CD-ROM drive to be

analyzed. However, it was found that switching to a braking mode at runtime was complicated and it also interfered with the tray mechanism of the CD-ROM drive. The details about braking modes are therefore not relevant to the scope of topic here and have been left out.

### **3.3 Materials**

The disposable disc is the heart of the Lab-On-CD device. Different materials and methods have been used to obtain microchannels on disc like structures. The most common materials used are Polymethyl-methacrylate (PMMA) and Polydimethylsiloxane (PDMS), however other materials like Polycarbonate and PVC have also been shown to yield satisfactory results. Some groups have also tried to bond PDMS chips onto a separate CD structure and used scotch tape to seal the channels.

In this thesis, initially standard polycarbonate plastic discs with metal and lacquer coatings were used. However, it was difficult to see the fluid flow with the coatings on the disk. Hence, clear, uncoated polycarbonate plastic discs were used later for the subsequent experiments. This also eliminated any effects the coatings might have on the flow properties and the fluid contact angles. Finally, compressed acrylic (also known as Lexan) discs were also used for the experiments since they were easily available and easy to machine.

### **3.4 Rapid Prototyping Method**

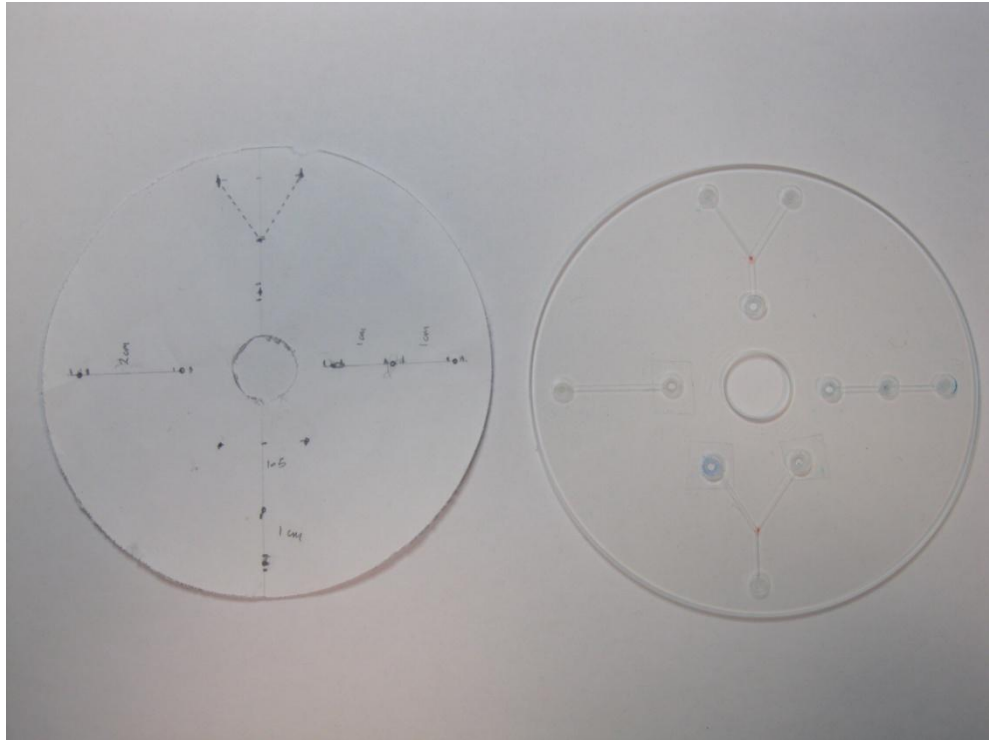
Typically, CNC machining or laser printing is used to make microchannels on polymer disks. Microfabrication techniques like deep reactive ion etching (DRIE) and wet etching can be used to make high-aspect ratio geometries. However, all of these technologies are costly, required elaborate preparation and long production times. The microfabrication process for polymers has been shown to be somewhat accelerated by

the use of positive microfabricated SU-8 masks which could be used multiple times to make geometries in polymers like Polydimethylsiloxane (PDMS) [5]. However, the mask still needs to be microfabricated and a limited number of variations of the geometry can be produced at a time.

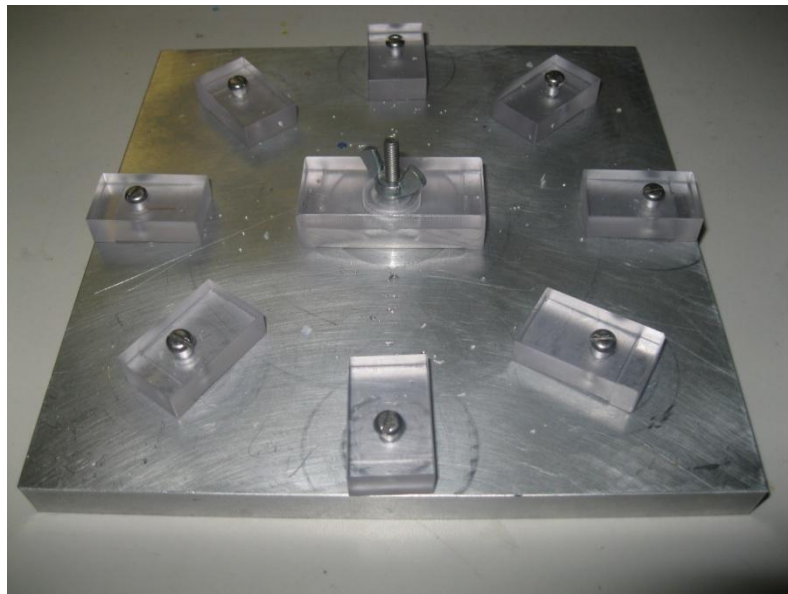
An innovative and rapid prototyping method was created and used to construct the channels and other geometries required for the experiments. This method was adapted from the traditional microfabrication method used in the manufacture of Micro-electro-mechanical Systems. The outline of the compact disk along with the center hole was sketched out on paper. The center of the concentric circles was found geometrically. Then distances from the center of the disc to the beginning of the reservoirs and the lengths of the channels were marked on paper. A pin-hole was made at the center of each of the reservoirs outline on the mask by using a sharp object like a pencil. Figure 3.4 shows a sample mask used to make the geometry for the basic experiments discussed later in Chapter 4.

A specialized vice was developed to hold the disk and the mask in place. This assembly contained a central nut-bolt fixing clamp along with other radial clamps. Figure 3.5 shows the specialized CD holder used in the rapid prototyping method. The mask was placed on top of the compact disc and a marker was used to mark the locations of the reservoirs in the geometry. The mask was then removed and a step-drill was used to machine the reservoirs on the CD. The final step was creating the channels by using a ruler and a carbide tip scribe pen.

The process has been continually optimized to get the best channel configurations. Initial attempts resulted in channels with highly serrated edges and were found to be too wide. Channels with smooth walls, appropriate uniform rectangular cross-sections and ease of machining were desired.



**Figure 3.4** Design mask used to fabricate the geometries on a CD.

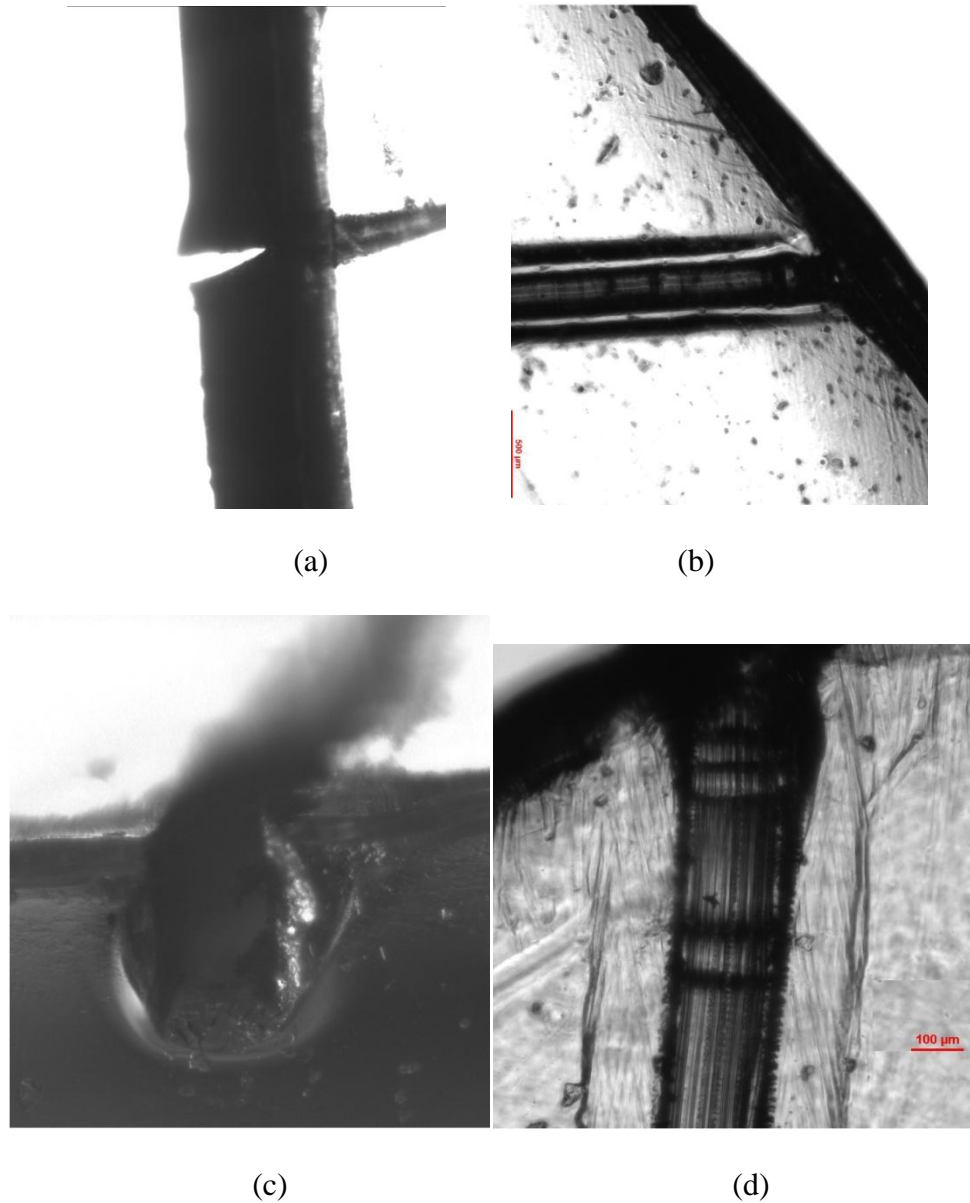


**Figure 3.5** Specialized CD holder used in the rapid prototyping method.

Initially, a simple blade having thickness  $290\text{ }\mu\text{m}$  was used to construct channels. The channels were found to have a triangular profile as shown in Figure 3.6(a). A rectangular profile was more desirable since it makes the equations for fluid



flow in micro-channels easier to use. The blade was therefore modified (machined) in order to create a rectangular and narrower profile. This yielded microchannels 250  $\mu\text{m}$  wide and 100-200  $\mu\text{m}$  deep. Figure 3.6 shows the different views of the microchannels under the microscope.



**Figure 3.6** (a) Micro-channel with triangular cross-section, (b) Width = 290  $\mu\text{m}$ , (c) rectangular cross-section obtained by modifying the blade, (d) channel width = 250  $\mu\text{m}$ .

After preliminary experiments, it was found that 250 micro-meters was not the optimum width for channels. Since blood cells are of the order of 6-20 micro-meters,



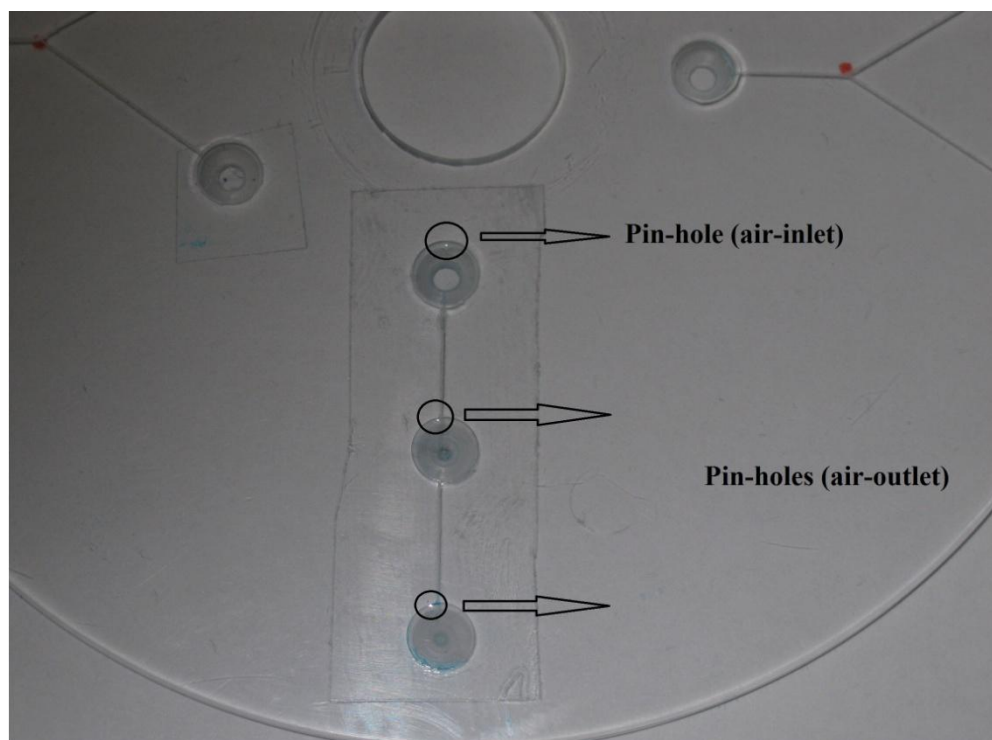
channels with smaller dimensions were required. Another factor influencing the width of the channels was the maximum rpm required for separating different components of blood. Theoretical calculations have shown that the rpm required for separating a 10 micro-meter particle (for example a red blood cell) is about 7000 rpm (Refer Appendix A).

Other approaches such as hot-embossing and machining were tried but the resulting channels were found to be too wide or not smooth respectively. Finally, channels were made by using a scribe pen with a carbide tip of 75 micrometers diameter. The scribe pen created satisfactory channels which did not leave a 'lip' on the surface of the CD. This eliminated any leakage of fluid from the surface of the CD. The channels were assumed to have a square or rectangular cross-section for the purpose of theoretical calculations but practically they were found to have trapezoidal profiles. Also, channel depth was assumed to be uniform but practically it was difficult to maintain a uniform channel depth by controlling the pressure on the scribe pen.

### **3.5 Sealing Methods**

Sealing the microchannel geometry to avoid leaking of fluids is a major concern in microfluidic chip design. Different types of sealing methods have been used for different purposes. Some groups have bonded two discs made of PDMS or PMMA together by applying the right combination of heat and pressure. Others have simply used transparent scotch tape to seal the channels to make them washable and reusable. Clear Scotch tape was also used in this thesis to seal the microchannels so that the flow can be examined by the naked eye and the channels could be reused after washing/rinsing.

An important consideration to be made while sealing the microchannels was to provide an outlet for the existing air inside the microchannels and reservoirs. This was required in order to relieve the air pressure to maintain a large pressure gradient. If such an outlet was not provided it was observed that opposing air pressure developed was strong enough to prevent the regular flow of liquid. Similarly, it was also found that the reservoir initially containing the sample also required an air inlet to avoid the development of negative pressure build-up (or a small vacuum). The inlet needed to be placed strategically such that no liquid leaked out of the reservoir. Therefore, to overcome these problems with sealing a small pin-hole was made strategically at the top-left of all reservoirs such that the collecting liquid would not flow out of the reservoir under the influence of the centrifugal and coriolis forces. Figure 3.7 shows a schematic of the reservoirs, sealing and the pin-holes made for allowing air to escape.



**Figure 3.7** Sealed reservoirs with pinholes as air inlets and outlets.

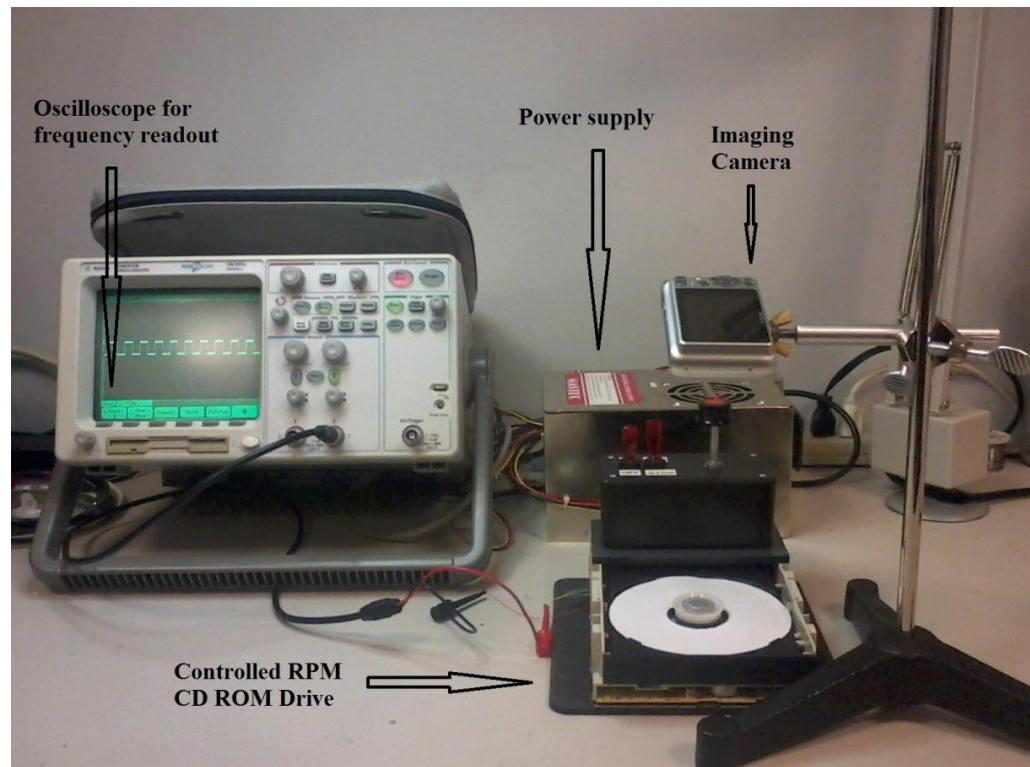
### 3.6 Complete Experimental Setup

The complete setup for performing the experiments shown in Figure 3.8 included the modified CD-ROM drive, an oscilloscope for measuring the frequency of rotation, a tripod stand and a fixture for a digital camera (Cannon Powershot A3100 IS). The camera was found to be able to capture images of the rotating disk at high speeds and therefore used extensively for this thesis. The modified CD-ROM was fitted with a project box to hold the rpm-control potentiometer and RUN/STOP and ON/OFF switches as shown in Figure 3.8(a). The tray holding the CD ROM was covered with white paper to give a good contrast background for the images captured. The 3-phase Brushless DC Motor Controller chip (TA 8493AF) discussed in Section 3.1 generates a square-wave signal on the  $f_{out}$  pin with a frequency proportional to the instantaneous rpm of the drive. The rpm of the CD-ROM is usually a simple multiple of this frequency and this information is mentioned in the datasheet for the chip. A digital oscilloscope (Agilent MegaZoom 54622A) was used to observe the instantaneous rpm of the drive. The multiplication factor between the output frequency and the actual rpm was also verified with a handheld digital tachometer.



(a)

**Figure 3.8** (a) A close-up of the modified CD-ROM.



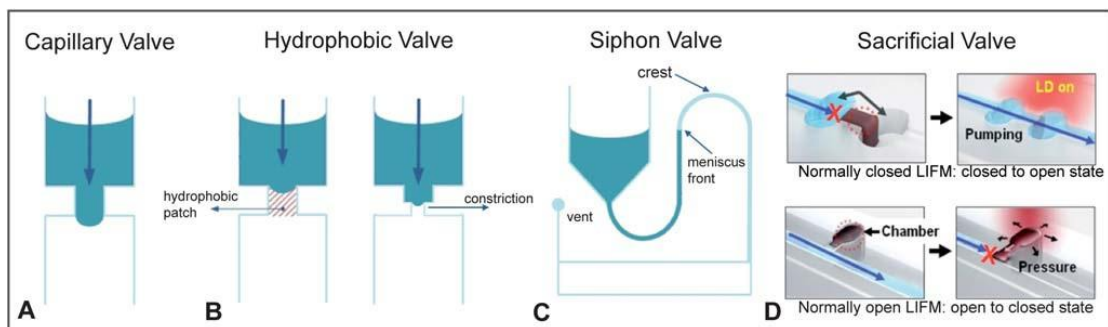
(b)

**Figure 3.8** (a) A close-up of the modified CD-ROM, (b) Complete experimental setup. (Continued)

## CHAPTER 4

### EXPERIMENTS AND PROTOCOLS

The control of flow of liquid is an essential task in any microfluidic system. Careful control of pumping and valving events is required which is a challenge in microfluidic systems. One way of achieving this is by rotating a disk at controlled angular velocities. However, pumping control alone is insufficient for analysis systems and simple reliable valves are required for accurately controlling fluid flows in microfluidic networks. Conventional diaphragm valves with or without moving parts or external actuation mechanisms often complicate the design and implementation[22]. The rotating nature of the device makes it impractical to use active flow-control mechanisms like electric/magnetic fields or other active valves or pumps. Hence, only passive components such as valves can be used for flow control. This Chapter explores the design of such passive valves for fluid stop-release function, flow switching and flow mixing. The common valves used in centrifugal microfluidics are depicted in Figure 4.1.



**Figure 4.1** Different valves used in centrifugal microfluidics. [2]

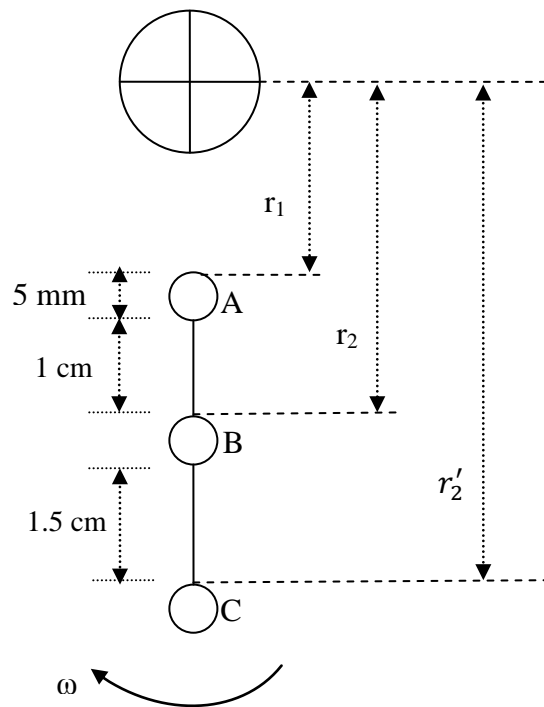
Hydrophobic, siphon and sacrificial valves have been used successfully for gating fluid by some groups. However, each type of valve has its limitations: hydrophobic valves are susceptible to introducing bubbles in the flow, siphon and

sacrificial valves are difficult to design, and sacrificial valves require external heating mechanism like a laser to actuate the valve. In this thesis, the capillary valve has been used exclusively for its simplicity of design and ease of fabrication and theoretical analysis.

#### **4.1 The Capillary Burst Valve**

Passive microfluidic capillary driven valves that exploit the surface tension force to stop the flows in microchannels have been a good alternative to the conventional valves. These passive valves do not require any moving parts and are not sensitive to the chemical properties of the sample fluid and do not face problems such as joule heating which occur in electrokinetic systems. A capillary valve gives good stop-release functionality and operates on the pressure barrier that develops when the cross section of a capillary expands abruptly. The liquid flowing in the channel is stopped by the drop formed due to surface tension at the end of the capillary. The pressure due to surface tension is known as the capillary barrier pressure and the pressure being exerted on the liquid due to the centrifugal force is called the meniscus pressure.

Capillary valves have been used and analyzed extensively in [22], [26], [27], for gating fluid flows. The first experiment that was carried out for this thesis was to verify the burst valve frequency required to overcome the capillary forces on the liquid in a microchannel and establish the parameters for the experiment. The verification of the required burst valve frequency was carried out by using a simple geometry as shown in Figure 4.2.

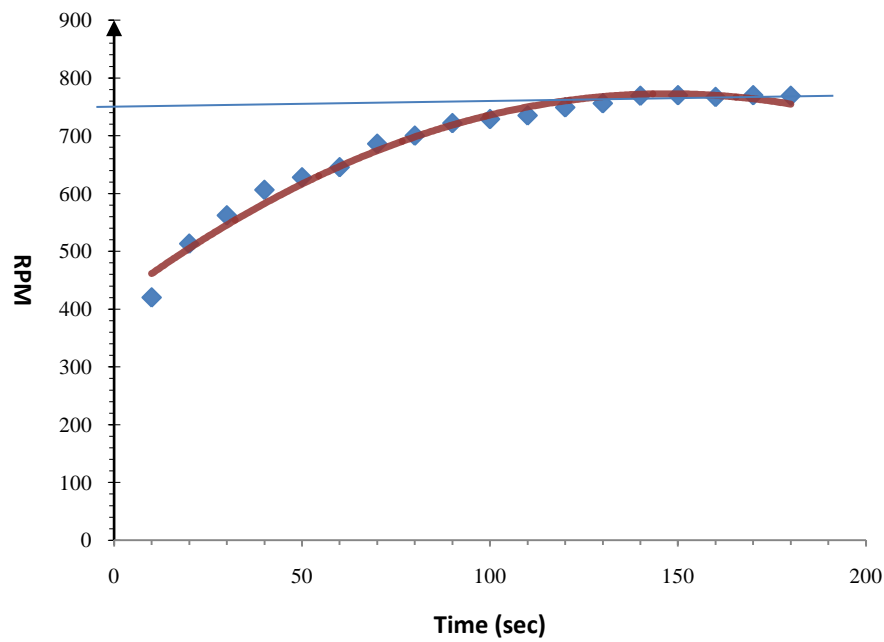


**Figure 4.2** Geometry to verify the Burst Frequency Equation.

The geometry was constructed by using the prototyping method discussed in Chapter 3. In Figure 4.1 the reservoir A is near the center of the disc and reservoir C is near the edge of the disc. The distances denoted by  $r_1$ ,  $r_2$ ,  $r_2'$  are used in the calculations of the capillary burst frequency in Section 4.1.1. All of the reservoirs and channels were sealed with ordinary clear Scotch tape. Breather holes were created for all reservoirs at the edge nearest to the center of the disk to provide pressure relief as discussed in Section 3.5.

Initial experiments showed that the CD-ROM could not be set during the actual experiment since the device had a tendency to overshoot the desired rpm values. Hence a different protocol was followed where the desired rpm was first set using a stock CD and then without moving the potentiometer the device was stopped using the RUN/STOP switch. Then the CD containing the sample was loaded on the

motor and the RUN/STOP switch was flipped to start spinning the disk again. It was observed that it took  $90 \pm 30$  seconds for the device to reach the preset rpm when starting from rest. Hence, the measurement of the spinning time was started only after the rpm reached the desired value. A graph of the rpm versus time in seconds is plotted in Figure 4.3 to show the response time of the CD-ROM device to reach 750 rpm.



**Figure 4.3** Graph of RPM versus time in seconds.

#### 4.1.1 Derivation of the Critical Capillary Burst Condition

The critical condition for the capillary burst frequency can be derived by first considering the pressure of the liquid column from reservoir A (Figure 4.2) to the capillary valve before reservoir B. From the Bernoulli equation, the pressure difference at the two ends of a channel can be given by:

$$P_1 + \frac{1}{2}\rho\omega^2 r_1^2 = P_2 + \frac{1}{2}\rho\omega^2 r_2^2$$

where,



$\rho$  = Density of the fluid

$\omega$  = Angular Velocity

$r$  = average distance of the liquid element from the center of rotation

$\Delta r$  = radial length that the liquid sample occupies

$\gamma_{al}$  = Surface tension of the fluid

$\theta_c$  = Equilibrium contact angle

$D_h$  = Hydraulic diameter of the channel

$P_1$  = Pressure at the top of the liquid meniscus in reservoir A

$P_2$  = Pressure at the end of the liquid column at capillary valve B

The difference in pressure at points 1 and 2 can be denoted by:

$$\Delta P = \frac{1}{2} \rho \omega^2 (r_2^2 - r_1^2)$$

$$\Delta P = \frac{1}{2} \rho \omega (r_2 - r_1)(r_2 + r_1)$$

Rearranging,

$$\Delta P = \rho \omega (r_2 - r_1) \left( \frac{r_2 + r_1}{2} \right)$$

$$\Delta P = \rho \omega^2 \Delta R \bar{R}$$

where,

$\Delta R$  = length of the liquid column

$\bar{R}$  = average radius from the center of rotation

Note that for calculating the burst frequency for the valve at C the values used

will be  $\Delta R = r_2' - r_2$  and  $\bar{R} = \frac{r_2' + r_2}{2}$

The Burst Frequency equation for a given microchannel is given by:

$$\rho \omega^2 r \Delta r < \frac{4 \gamma_{al} \sin \theta}{D_h}$$

where, the left hand side denotes the Meniscus Pressure and the right hand side denotes the Capillary Barrier Pressure.

Since the above formula assumes an axis-symmetric capillary with a circular contact line a correction factor was found by Zeng et al. to yield better conformance with experimental burst frequency values [27]. Burst frequencies have been shown to be dependent on cross sections for channels with equal hydraulic diameters. A correction factor has been added to the theoretical burst frequency equation as follows to account for the variation in channel cross section.

$$\rho\omega^2r\Delta r < \frac{4\gamma_{al} \sin \theta}{D_h^n}$$

Where  $n = 1.08$  for equilateral triangular cross-section and  $n = 1.14$  for rectangular cross sections. Additional modification required in case of pipe flow has been described in [26-27].

#### 4.1.2 Calculation of Theoretical Values

The verification of the burst frequency for the valves at B and C (refer Figure 4.2) was carried out with both water color and blood. For calculating the theoretical values for the burst frequencies with water color the surface tension was experimentally measured using a glass capillary tube method. Microhematocrit tubes made by Jorgensen Laboratories Inc. Loveland CO, part number J-543 are used for the surface tension calculations. The air-liquid surface tension is directly proportional to the height to which the liquid rises in the capillary tube. The liquid-air surface tension is given by

$$\gamma_{al} = \frac{h\rho gr}{2 \cos \theta}$$

where,

$h$  = height to which the liquid rises in the tube

$\gamma_{al}$  = liquid-air surface tension

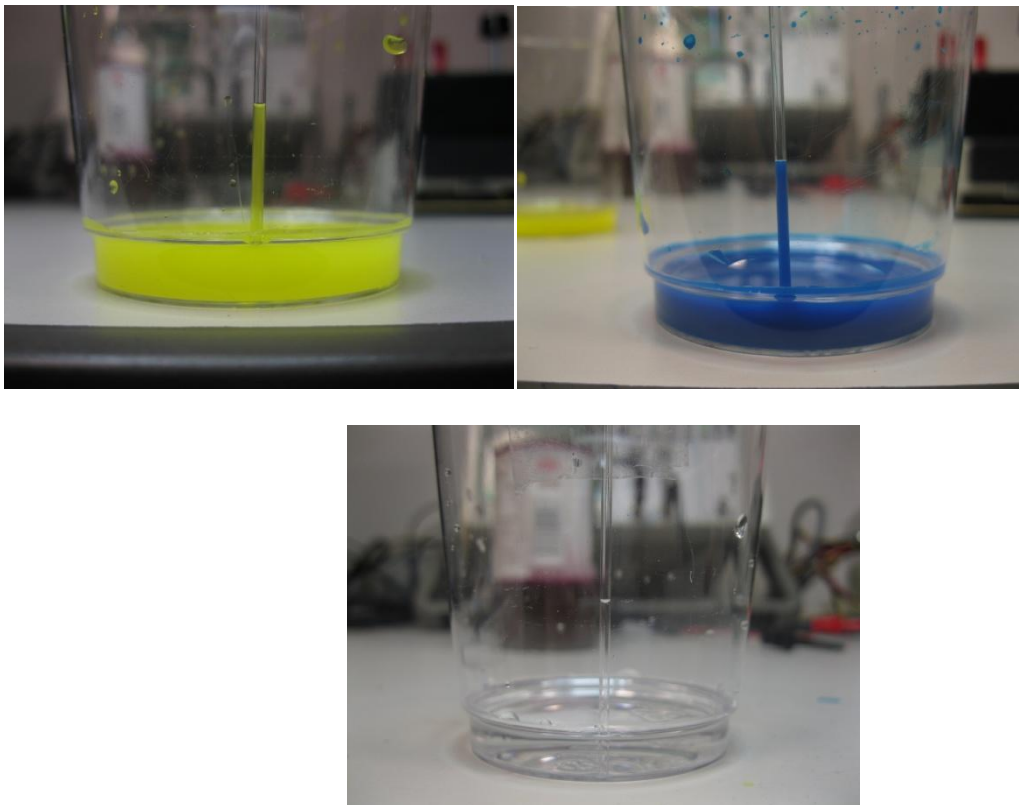
$\rho$  = density of the liquid

$r$  = radius of the capillary

$g$  = acceleration due to gravity

$\theta$  = contact angle (assumed to be maximum  $0^\circ$ )

In order to determine the surface tensions of the different water colors used for the experiment, each color liquid was poured in a container to a height of 7 mm and a glass capillary was held upright in the liquid. Once the liquid rose in the capillary, the other end was sealed and the height of the liquid in capillary was measured. Figure 4.4 shows the experiments carried out to determine the surface tension of different water colors with respect to water.



**Figure 4.4** Surface tension measurements of different water colors and water.

The liquid-air surface tension of water at 25° C is known to be 72 mN/m. The calculated value for the surface tension of water was 70.44 mN/m which compares well with the theoretical value. The calculated value for the surface tension of the yellow color is 61.31 mN/m and for the blue color it was found to be 67.62 mN/m. The theoretical burst frequencies were calculated based on the surface tension value for blue color since it was used for this set of readings.

Initially, the reservoir A was filled up with a water-based dye and the disc was made to spin for 15 second intervals (spinning time) at increasing rpm's of steps of 10 rpm per interval to check if the liquid flowed from reservoir A to B. The measurement of the spinning time was started only after the rpm reached the desired value. The parameter values used and theoretical values calculated for valve at B are shown in Table 4.1.

**Table 4.1** Capillary Burst Valve Parameters for Valve at B

Parameter	Values for water color	Values for blood
R1 (cm)	2.3	2.3
R2 (cm)	3.6	3.6
Width of Channel ( $\mu\text{m}$ )	200	200
Depth of channel ( $\mu\text{m}$ )	170	170
Contact Angle (degrees)	90	90
Surface tension (N/m)	72	55.89
Fluid Density ( $\text{kg/m}^3$ )	1000	1060
Theoretical Burst Freq (RPM)	591.74	522.54
Theoretical Burst Freq with Correction Factor (RPM)	1115	954.2

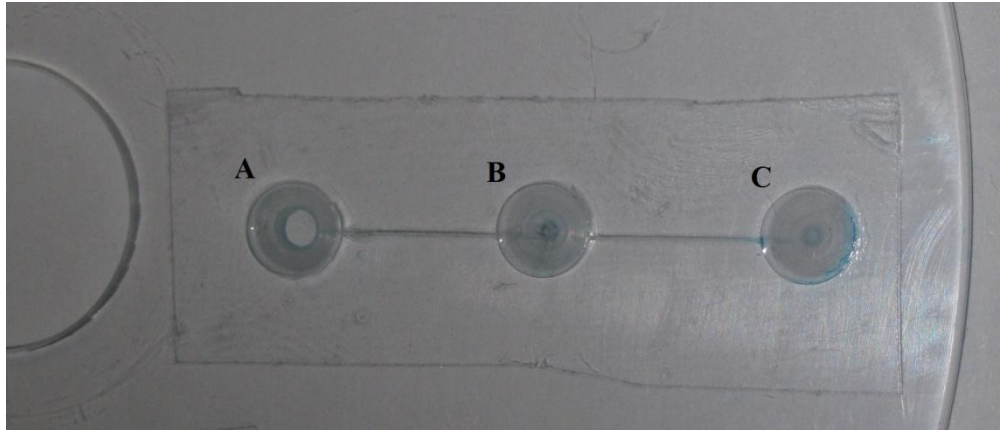
Similar verification of burst frequencies was also carried out for the valve at C. The parameter values used and theoretical values calculated for valve at C are

shown in Table 4.2 below. Since the fluid element is located further away from the center of rotation the apparent tangential velocity at C is also higher.

**Table 4.2** Capillary Burst Valve Parameters for Valve at C

Parameter	Values for water color	Values for blood
R1 (cm)	3.6	3.6
R2 (cm)	5.1	5.1
Width of Channel ( $\mu\text{m}$ )	200	200
Depth of channel ( $\mu\text{m}$ )	170	170
Contact Angle (degrees)	90	90
Surface tension (N/m)	72	55.89
Fluid Density ( $\text{kg/m}^3$ )	1000	1060
Theoretical Burst Freq (RPM)	453.8	400.68
Theoretical Burst Freq with Correction Factor (RPM)	855.08	731.68

Although the theoretical burst frequencies at C were lower than the burst frequencies at B, the fluid was successfully gated at B since the model considered for the analysis did not take into account the energy required to wet the walls of the reservoir B. It has been proved by Duffy et al. [15] that the energy loss occurring due to this plays a significant role if there are a series of valves and reservoirs along a single channel. A similar geometry has been used to demonstrate multi-step valves using a different rapid prototyping methodology in [25]. Figure 4.5 shows the geometry used to demonstrate gating of fluid using capillary valves.



**Figure 4.5** Geometry used to show gating of fluid (water-color and blood) using capillary valves.

This experimental protocol was followed for the verification of the critical burst frequency for both valves (at B and C). An important experimental observation was that the range of capillary stop conditions is dependent upon physical dimensions of the channels and reservoirs. This meant that a limited range of stop conditions could be obtained from a fixed geometry. If special stop conditions were desired then other means of stopping fluid flow would have to be explored. Hydrophobic coatings can be combined with capillary valves to give higher ranges of stop conditions without varying the geometry of the channels. However, hydrophobic coatings make the flow in the channel susceptible to air pockets which often cause failure in microfluidic systems [19].

## 4.2 Effects of the Coriolis Force

Capillary burst valves can only be used to stop/release the flow of liquid but there still remains a demand for more sophisticated and versatile valves which can perform complex microfluidic functions. A flow-switching valve is one such valve which controls the direction of liquid flow at a junction comprising of a common inlet and two outlet channels. It is very often combined with a capillary valve discussed in 4.1

to stop/release the flow of liquid. Flow-switching valves have been used in absorbance and fluorescence immunoassays to detect absorbance of DNA on a silica matrix by Jitae Kim et al. in [19].

The flow-switching feature of the valve is performed due to a pseudo-force called the Coriolis Force. This force becomes apparent in centrifugal microfluidics and is directly proportional to the angular velocity of the disk and the radial distance from the axis of rotation. It is perpendicular to the centrifugal force and its direction depends on the rotational direction of the disk. If the Coriolis force is given by  $f_{cor}$  and the centrifugal force is denoted by  $f_{cen}$  then,

$$f_{cor} = -2\rho\bar{\omega} \times \bar{u}$$

$$f_{cen} = -\rho\bar{\omega} \times (\bar{\omega} \times \bar{r})$$

where,

$\bar{\omega}$  = constant angular velocity

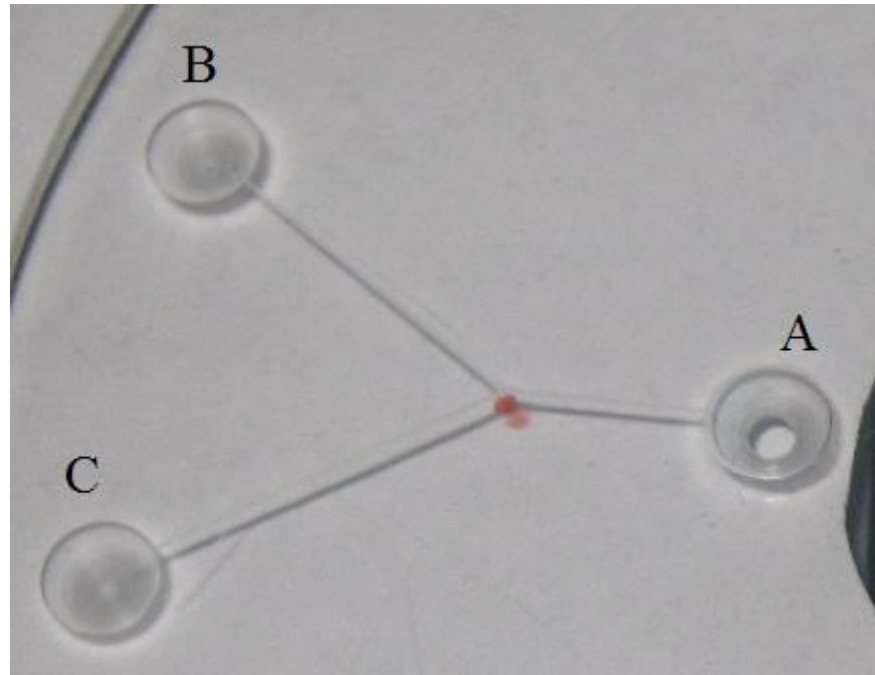
$\rho$  = density of the liquid

$\bar{r}$  = radial distance from the center of rotation

$\bar{u}$  = angular velocity at a distance  $r$

The Coriolis-to-Centrifugal force ratio has been found to be a linear function of the angular frequency of the disk and the aspect ratio of the channel cross-section. Flow switching valves and coriolis forces have been extensively analyzed in [19]. The geometry used to analyze the performance of the flow-switching valves is shown in Figure 4.3. For the purpose of this thesis the flow-switching valve has not been combined with a capillary burst valve before the location of the flow switching. The geometry was constructed by using the prototyping method discussed in Chapter 3. In Figure 4.6 the reservoir A is near the center of the disc and B and C are near the edge of the disc. All of the reservoirs and channels were sealed with ordinary clear Scotch

tape and then breather holes were created in the corners of all reservoirs to prevent any side-effects due to air pressure. Initially, the reservoir A was filled up with a water-based dye and the disc was made to spin for 15 second intervals at increasing rpm's of steps of 10 rpm per interval starting from 500 rpm to check if the liquid flowed from reservoir A to B or C.



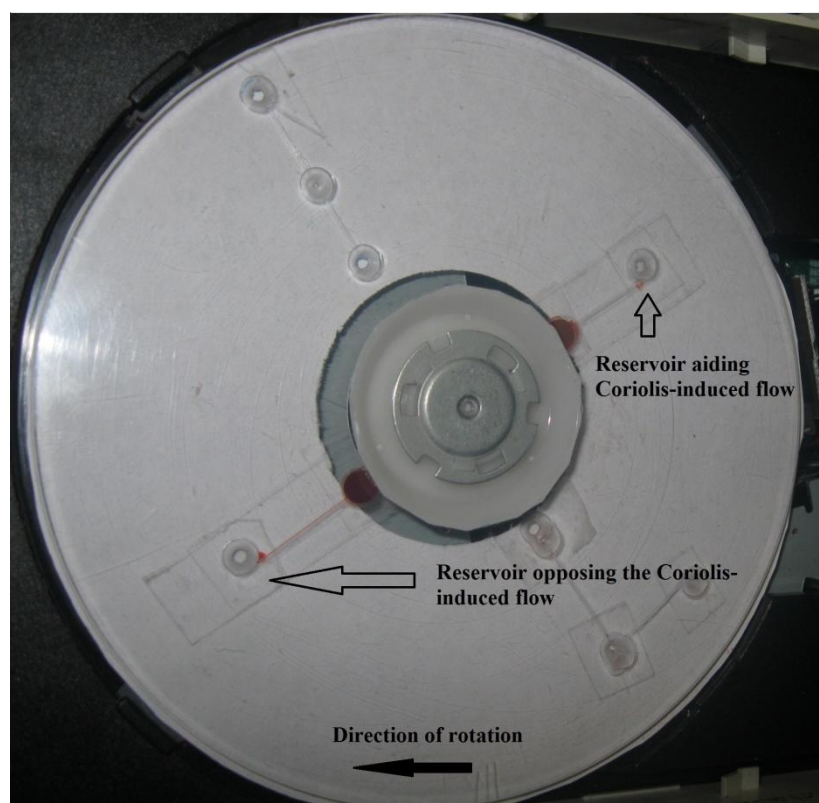
**Figure 4.6** Flow-switching valve on a CD.

The results of the flow-switching are analyzed and discussed in further detail in Chapter 5. A similar Y-channel configuration has been used by [20] to separate blood plasma from blood cells. However, the Coriolis Effect in a rotating frame of reference does not permit similar usage of the Y-channel. Hence, different configurations were tested for plasma separation from blood as discussed in Section 4.4.

Coriolis force can also be used in conjunction with capillary burst valves to gate the flow of liquid. The two geometries shown in Figure 4.7 were created by the rapid prototyping method mentioned in Chapter 3 and sealed with precautions for



pressure relief. The reservoirs near the center of the CD were loaded with anti-coagulated blood. Two target reservoirs towards the periphery of the CD were placed such that one reservoir would aid the flow due to the Coriolis force and the other would oppose such a flow. The samples were spun for fixed periods of time with an increment of 20 rpm/interval until the liquid in both valves burst through. The rpm at which each event occurred has been discussed further in Chapter 5.



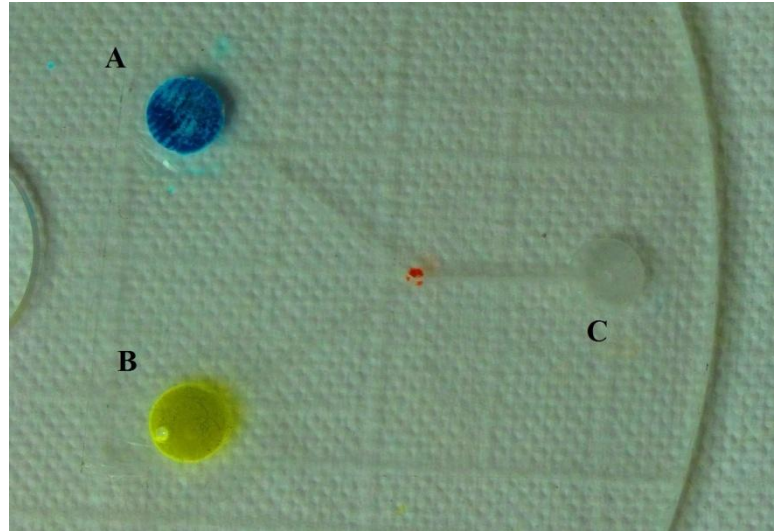
**Figure 4.7** Geometries used to verify the gating of fluid using the Coriolis force.

### 4.3 Mixing of Two Fluids in Microchannels

Most diagnostic assay protocols require mixing of two or more fluids (sample and reagents). Stopping and controlling flows has been successfully carried out in most microfluidic systems. However, mixing of two liquids still remains a major challenge. The primary reason for this is that the hydrodynamic conditions prevalent in flows through microstructures are strictly laminar. Therefore, turbulence formation by

means of either active or passive components is impossible, which means that diffusion is the primary mechanism of mixing. Since the rate of diffusion is directly proportional to the (microscale) dimension of the structure used for mixing and the time available for diffusion, it is not an efficient scheme for mixing fluids. Different schemes for mixing two liquids have been tested in centrifugal microfluidics. Moving parts or spatially varying fields have been explored to bring about mixing of fluids [7], [12], [16], [28]. In disk-based systems, frequent reversal of the sense of rotation have been used in conjunction with magnetic microbeads to mix microliter volumes of fluids. Passive mixing at low volume throughput has been explored by creating novel three-dimensional channel architectures and obstacles but they all rely on the pumping source for mixing energy. Multilamination schemes were developed to reduce mixing times and provide high volume throughput. Multilamination of flow implies creation of thin alternating lamellae of liquids which reduces diffusion length (due to thinness of the films) and eliminated the need for additional transversal flow components.

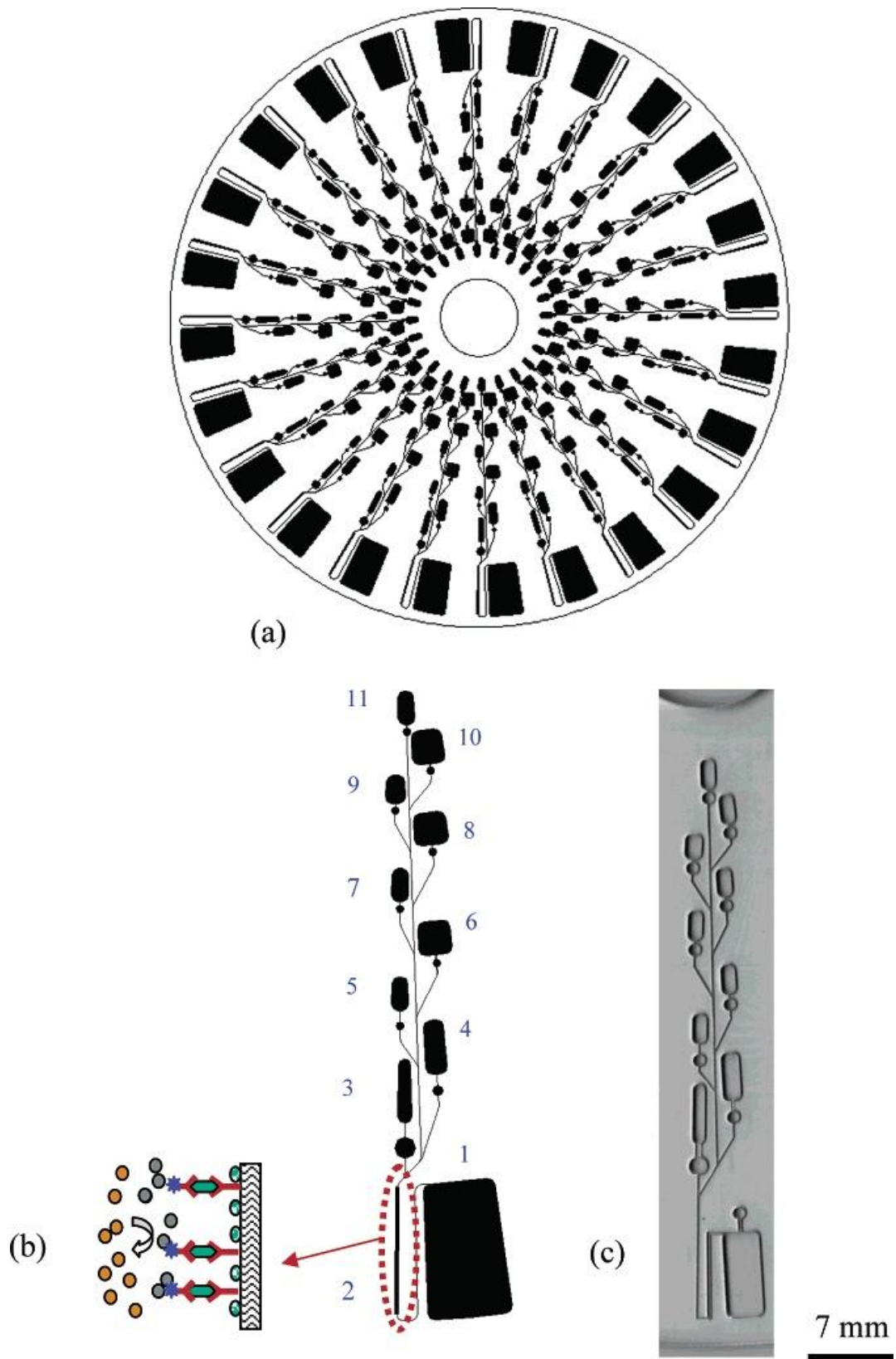
The geometry used to demonstrate mixing of two liquids in microchannels is shown in Figure 4.8. It was constructed by using the prototyping method discussed in Chapter 3. In Figure 4.8 the reservoirs A and B are near the center of the disc and C is near the edge of the disc. All of the reservoirs and channels were sealed with ordinary clear Scotch tape and then breather holes were created in the corners of all reservoirs to prevent any side-effects due to air pressure. Initially, reservoir A was filled up with a blue water-based dye and reservoir B was filled with yellow dye. The disc was then made to spin for 15 second intervals at increasing rpm's of steps of 10 rpm per interval starting from 500 rpm.



**Figure 4.8** Geometry used to test the mixing of two liquids in microchannels.

The objective of this experiment was to confirm the Coriolis-induced secondary flow pattern model as discussed in [7] and observe the degree of mixing. The detailed analysis and verification of the Coriolis-induced hydrodynamic reversal of the flow pattern has been carried out in [9]. A unique technique for mixing liquids was also reported by J. L. Garcia-Cordero et al. in [12].

Colorimetric assays have been created using centrifugal microfluidics by Steigert, Grumann et al. for detecting alcohol concentration and direct hemoglobin measurement on blood. Others have used the enzyme-linked immunosorbent assays (ELISA) for dengue, and fast detection of food based pathogens and toxins. Figure 4.9 shows the schematics of a CD design used in [8] to perform ELISA for rat IgG from hybridoma cell culture.



**Figure 4.9** Schematics of (a) CD-ELISA design with 24 sets of assays, (b) a single assay, (1 waste; 2 detection; 3 first antibody; 4, 6, 8, 10 washing; 5 blocking protein; 7 antigen/sample; 9 second antibody; 11 substrate) and (c) photo of a single assay. (Source: [8])

#### 4.4 Separation of Plasma from Blood

The separation of plasma from blood is often the first step in any blood analysis. Plasma proteins oppose the separating or sedimentation of cells in blood. Typically freshly drawn whole blood needs to be either de-fibrinated or anti-coagulated to prevent the formation of clots. De-fibrination is the process of removal of the plasma glyco-protein fibrinogen from blood typically using magnetic stirrers. Anti-coagulation on the other hand is a process where an anti-coagulant substance like a heparin or citrate compound to inhibit the conversion of fibrinogen into fibrin which in turn prevents coagulation (clot formation). Blood collected in testubes is generally anti-coagulated blood and it has been used for all the blood-related experiments in this thesis. Various geometries to separate plasma from blood were tested as described in the following sections.

##### 4.4.1 Simple Geometry with Capillary Burst Valves

The first trial was done using the geometry discussed in Section 4.1. It was observed that anti-coagulated blood generally started separating at around 1000 rpm as compared to whole blood which requires 3000-7000 rpm for separation. The model discussed in Appendix A was used to compute the frequency required to sediment red blood cells (8  $\mu\text{m}$  diameter) and white blood cells (12  $\mu\text{m}$  diameter). It was found that an rpm of 10,000 would be required to separate red blood cells and about 7000 rpm would be required to separate white blood cells. The difference in the observed values for separation and the calculated values was attributed to the change brought about by the anti-coagulant added to blood.

A capillary valve was fabricated to have a burst frequency around 1000 rpm to cause sedimentation of the blood and then separation based on the spinning time. The width and height of the resulting channels were 200 microns and 170 microns

respectively. Other parameters like radial distances and spinning times were kept same as those followed for the experiment in Section 4.1.

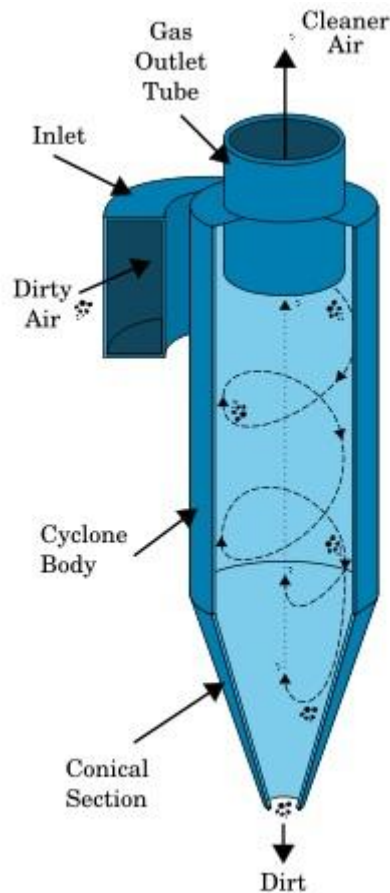
The geometry was loaded with anti-coagulated blood and the disk was spun for consecutive intervals of 10 seconds with rpm's incrementing in steps of 100 rpm. Periodic images were taken to see if the blood moved from reservoir A to B and to C. The results and conclusions are reported in Section 5.4.

#### **4.4.2 Using a Micro-Cyclone**

Another scheme that was experimented with was the implementation of the micro-cyclone concept for separation of plasma from whole blood. The concept was based on the use of cyclones for purifying air in pharmaceutical facilities. In pharmaceutical manufacturing facilities small particles from the drug powders are suspended in the air and remain in the air if they are not filtered out. Such particles pose a threat to those who work in such facilities and also contribute to the material loss. Hence, in order to keep a clean environment inside the facility and to reduce the wastage of materials a cyclonic air purifier is used as shown in Figure 4.10.

The cyclone separator uses rotational effects and gravity combined with flow-rates and optimized geometries to separate particles suspended in air. As shown in the figure, contaminated air is made to enter the chamber in a tangential manner to induce a high-speed rotating spiral flow at the top of the cyclone. The air flow ends at the bottom of the cyclone and the air exits in a straight upward fashion at the center of the cyclone through the top. The suspended particles strike the walls of the cyclone due to their inertia and lose momentum and fall to the bottom of the cyclone. The conical end of the cyclone reduces the rotating diameter of the air flow further thus causing increasingly smaller particles to separate out. This leaves purified air at the bottom of the cyclone which is made to exit straight up from the center of the cyclone. This

scheme of separation along with the correct cyclone geometry and a few other design modifications and cascading have been known to provide high (>90%) purification efficiencies. (Source: Rhodes M. (1998). Introduction to particle technology. John Wiley and Sons. [ISBN 0471984833](https://doi.org/10.1002/9781118483333))



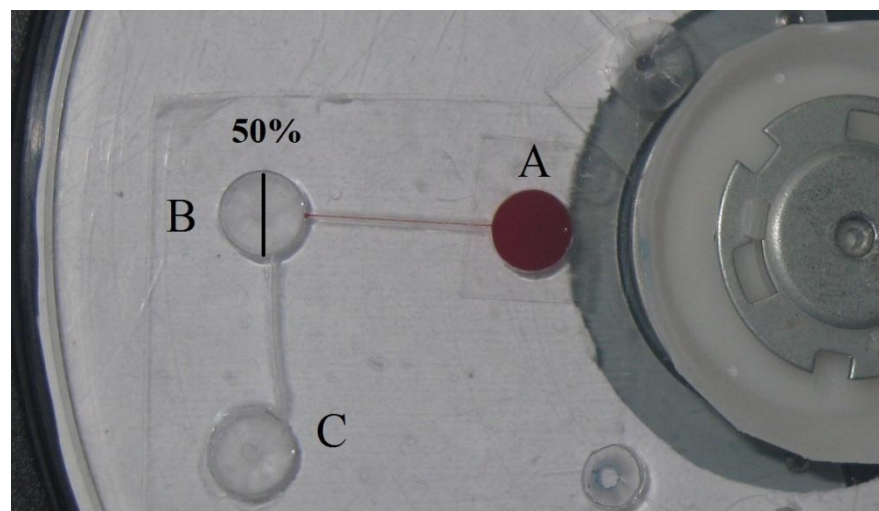
**Figure 4.10** Cyclonic air purifier employed in pharmaceutical industries. (Source: [http://en.wikipedia.org/wiki/Cyclone\\_separator](http://en.wikipedia.org/wiki/Cyclone_separator))

The implementation of the concept of the cyclone was attempted for separating out plasma from blood. The geometry was modified such that both sides of the disk were used to create the channels and reservoirs. The input reservoir and inlet channel was made on the top of the CD leading into the cyclone which spanned the entire thickness of the CD (2 mm). The upper diameter of the cyclone was 6 mm and the lower diameter was 2 mm. An outlet for the waste (red-blood cells) was made at the bottom and another outlet for the plasma was made at the top of the CD. Different

variations of this scheme of directing the flow through the substrate and placing the outlets at strategic points were tried. However, after testing the initial prototypes it was found that, in a rotational system the interplay of centrifugal and coriolis forces did not permit the spiral-flow pattern which is the building block of the cyclone. Therefore no further testing was conducted for this type of geometry.

#### 4.4.3 Using an Accurate Metering Geometry

The percentage composition of blood shows that 50-55% of blood is plasma. There are minor variations according to species, and sex but the normal hematocrit range for humans, canines and felines are well established. Hence, if the starting volume of blood is known then it can be safely assumed that about 50% of it will be plasma. The exception to this would be if the blood came from a diseased person or animal. Using this concept a separation and metering geometry as shown in Figure 4.11 was created for separating plasma from blood.

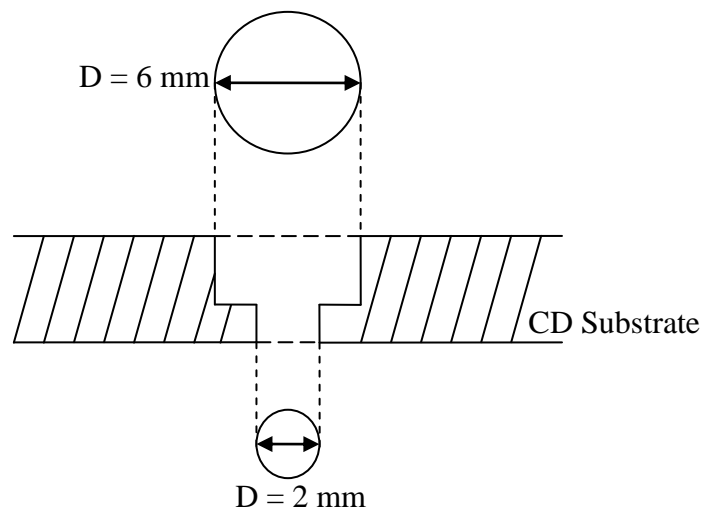


**Figure 4.11** Separation and metering geometry for plasma separation.

The geometry was created using the rapid prototyping method mentioned in Chapter 3. The channels and reservoirs were sealed with transparent Scotch tape and breather holes were created in order to eliminate any effects of trapped air in the



reservoirs or channels. Initially, a cylindrical input reservoir (A) of 6 mm diameter was milled to a depth of 1.15 millimeter. Then a smaller, concentric cylindrical hole was made through the remaining substrate to serve as an inlet for the liquid. The geometry of the input reservoir A is shown in Figure 4.12. The total volume of liquid that this reservoir could hold was calculated from geometry to be 34.054  $\mu\text{L}$ . An equal-volume reservoir (B) was made towards the periphery of the disk to serve as the separation chamber. A third reservoir (C) was created at a different radial location as shown in Figure 4.11. This reservoir was meant to serve as the output reservoir where clear plasma would be collected. The volume of this reservoir can be modified to meter the required amount of plasma from blood. Reservoirs B and C were connected by a strategically placed radial channel. The placement of this channel is crucial in determining the percentage volume of plasma that will be removed from reservoir B and transferred to reservoir C due to Coriolis force. The channel was initially placed such that it would allow about 50% of the volume of reservoir B to flow into the (plasma collection) reservoir C.



**Figure 4.12** Geometry of the input reservoir.

The input reservoir of the sealed geometry was filled with anti-coagulated blood and the disk was made to spin at 1000 rpm for 15 seconds. Thereafter the rpm was increased to 3500 rpm in steps of 100 rpm every 5 seconds to check if the separated blood flowed into reservoir B. Reservoir C received clear plasma flow after about 60 seconds of spinning due to the coriolis induced pressure in reservoir B. The separated plasma was also analyzed separately for presence of any white blood cells by regular staining procedure on a glass slide.

## CHAPTER 5

### RESULTS AND DISCUSSION

#### 5.1 Capillary Burst Frequency

The geometry discussed in Section 4.1 was used for the verification of the capillary burst frequency. The capillary burst condition was used to calculate the critical burst frequency theoretically. Rearranging the terms of the equation derived in Section 4.1.1,

$$\rho\omega^2 r \Delta r = \frac{4\gamma_{al} \sin \theta}{D_h}$$

Representing the right hand side of the equation as the capillary pressure due to surface tension  $P_c$ , the critical burst frequency can be written as,

$$\omega^2 = \frac{P_c}{\rho r \Delta r}$$

Taking square-root of both sides,

$$\omega = \sqrt{\frac{P_c}{\rho r \Delta r}}$$

The relation between angular velocity  $\omega$  and revolutions per minute is given by:

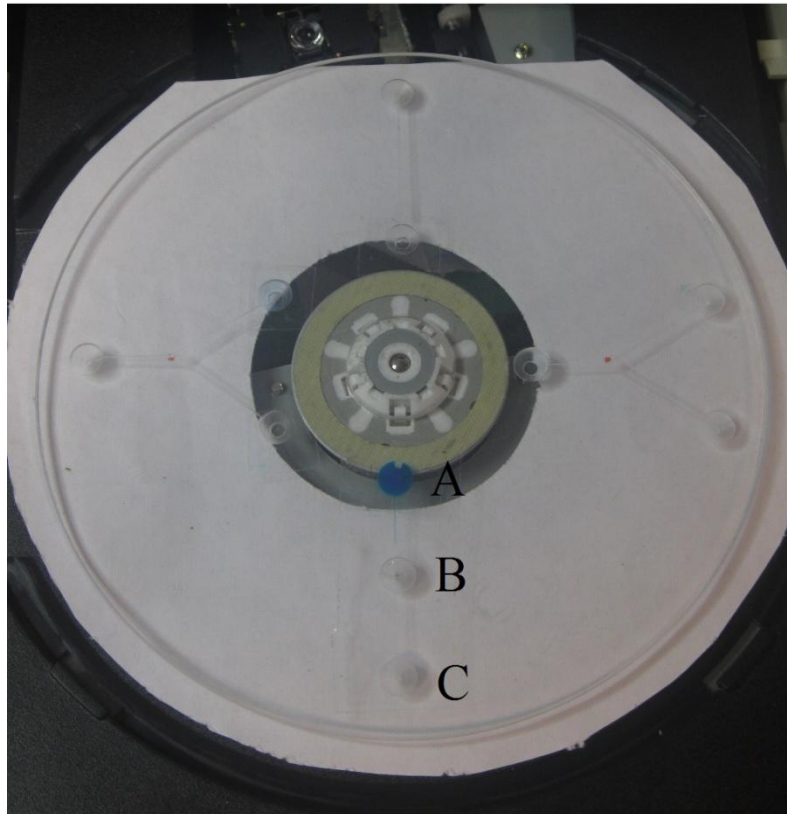
$$\omega = \frac{2\pi f}{60}$$

since a minute has 60 seconds. Therefore rearranging and substituting in the square-root equation derived in the earlier step,

$$f = \frac{30}{\pi} \sqrt{\frac{P_c}{\rho r \Delta r}}$$

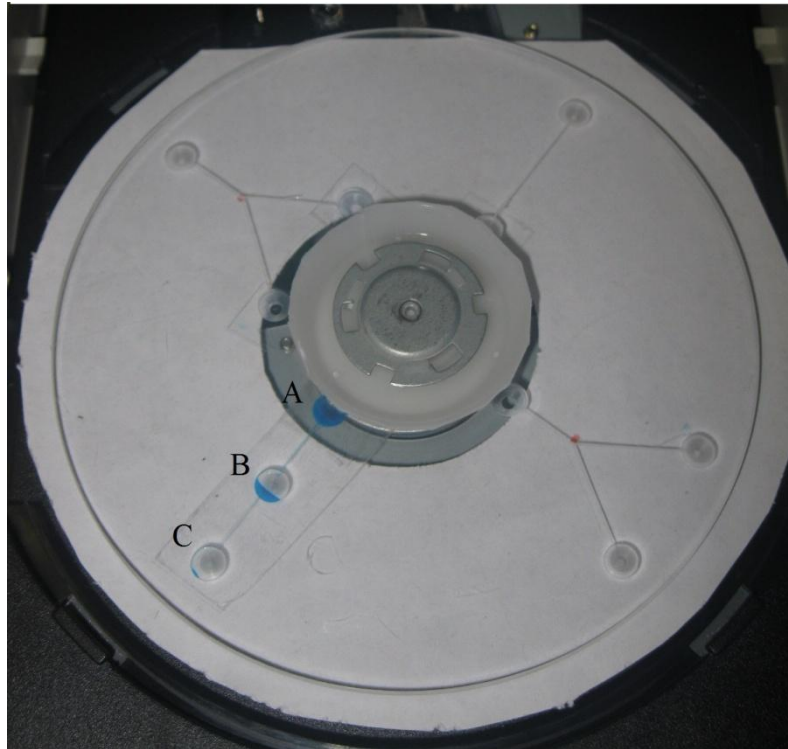
Using the equation above, theoretical values for the burst frequency were calculated based on the measured geometric dimensions and the calculated values for

surface-tension etc. The correction factor for the hydrodynamic diameter for rectangular cross-section channels derived in [27] was also applied and the resulting values were recorded as the upper limits for the burst frequencies. Figure 5.1 shows the photographs of the steps in the verification of the burst frequency for valve at B.

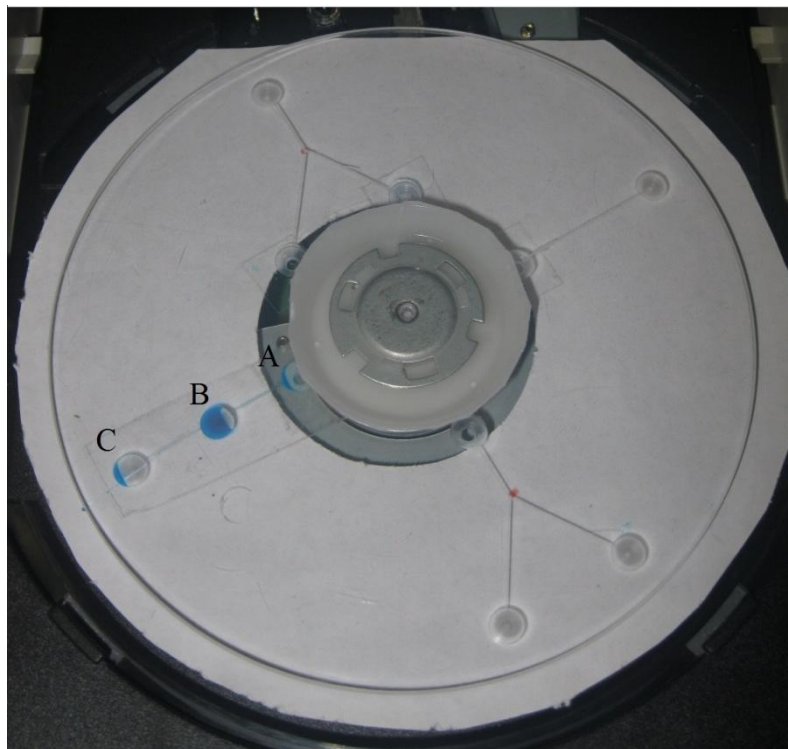


(a)

**Figure 5.1** Verification of capillary burst frequency carried out with water color (a) input reservoir loaded with water color.



(b)



(c)

**Figure 5.1** Verification of capillary burst frequency carried out with water color (b) water color burst into reservoir B, (c) water color burst into reservoir C. (Continued)

Table 5.1 presents a comparison of the theoretical and observed values for the capillary burst frequencies for blue water color.

**Table 5.1** Comparison of the Theoretical and Observed Values of the Critical Burst Frequencies for Water Color

Valve at B			Valve at C	
	Theoretical	Observed	Theoretical	Observed
RPM Without Correction Factor	591.74	840 ± 20	453.8	680 ± 20
RPM With Correction Factor	1115.4		855.08	
Inside the range?	Yes		Yes	

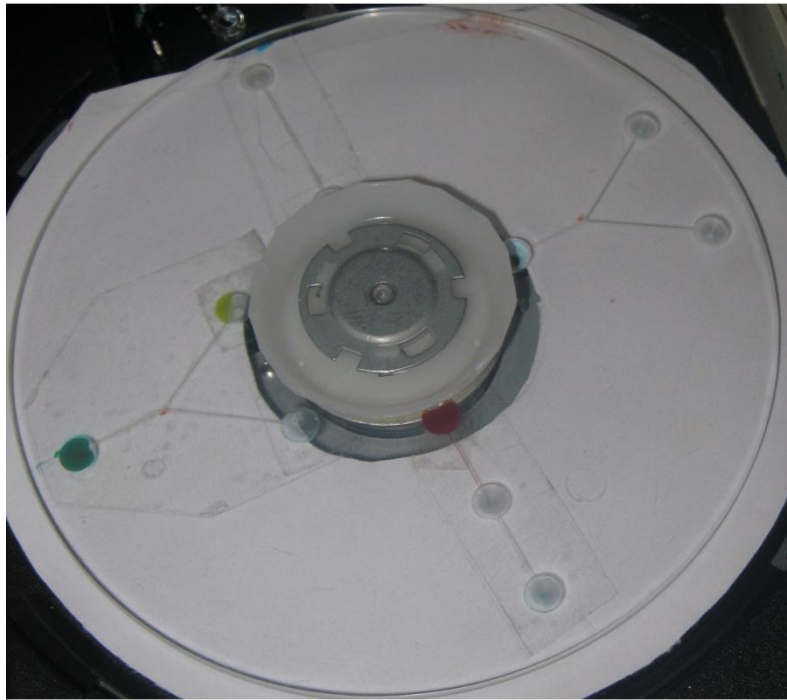
The observed values of burst frequencies show good conformance with theoretical values. The difference between the theoretical and observed burst frequency values at B can be attributed to the errors in measuring the channel dimensions, error in reading the actual instantaneous rpm of the disk, and contact angle of the liquid with the surface of the disk. The channel profile has also been approximated to be a rectangular cross-section when in-fact it has been observed to be trapezoidal in nature. This is caused due to the trapezoidal profile of the tip of the scribe pen used to make the channels. However, the error in the rpm is not significant and therefore capillary valves can be successfully used to gate the flow of fluid in centrifugal microfluidic applications.

The same valves were also tested with anti-coagulated dog blood collected in a collection tube. Theoretical values for burst frequency rpm were calculated for blood using corresponding values for surface tension and viscosity and then compared with the experimental results as shown in Table 5.2.

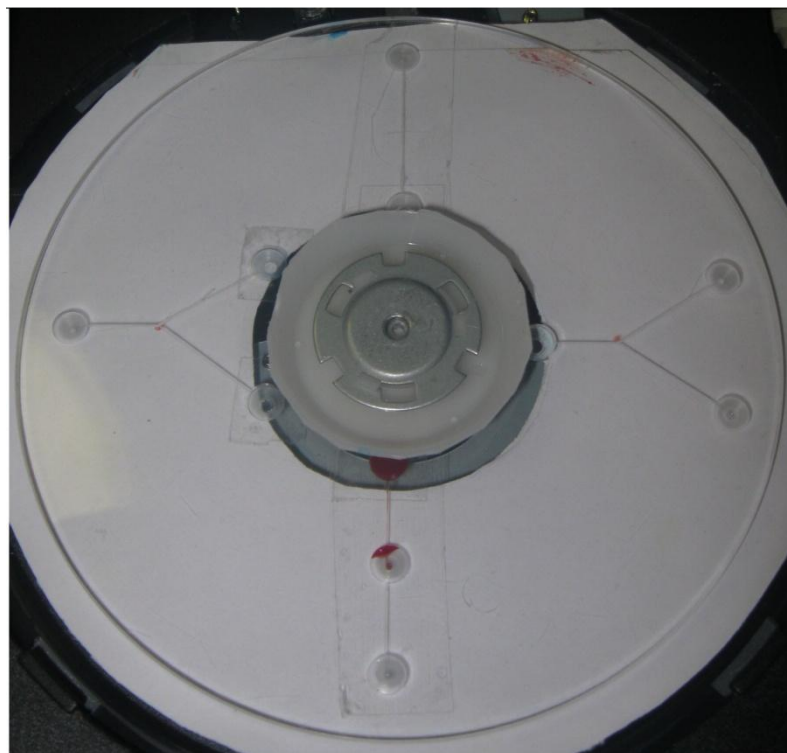
**Table 5.2** Comparison of the Theoretical and Observed Values of the Critical Burst Frequencies for Anti-Coagulated Blood

Valve at B			Valve at C	
	Theoretical	Observed	Theoretical	Observed
RPM Without Correction Factor	522.54	760 ± 20	400.6	600 ± 20
RPM With Correction Factor	954.2		731.68	
Inside the range?	Yes		Yes	

The theoretical and observed values of burst frequencies were lower for blood as compared to the water color. This result was due to the fact that blood has lower surface tension than the water color. The observed values of the burst frequencies show good conformance with theoretical values. In addition to the factors that cause errors in estimating the burst frequency of the valves anti-coagulated blood presents its own set of errors and problems. Factors like the hematocrit level and number of days since the blood was drawn contribute adversely to the measurements. It was observed that even at low rpm's anti-coagulated blood starts separating into plasma and cellular pellet. This cellular pellet is mostly made up of solid cells which tend to block the tip of the channel and cause the 'burst' to occur at a higher rpm. However, this phenomenon can also be used as a potential mechanism of separating plasma from blood. With accurate control of rpm's and spinning times it has been shown in Section 5.4 that plasma can be separated from blood using only capillary valves.



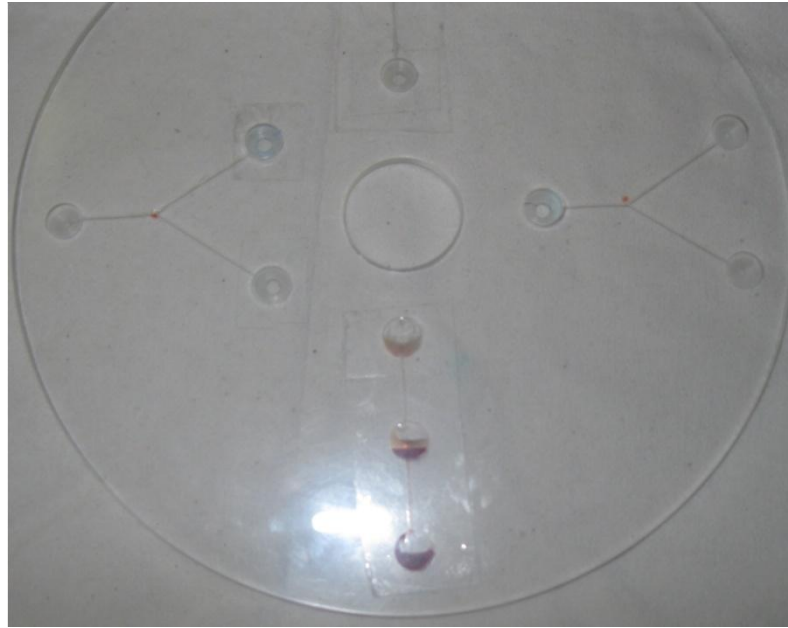
(a)



(b)

**Figure 5.2** Verification of capillary burst frequency carried out with blood  
(a) Input reservoir loaded with blood, (b) blood burst into reservoir B.





(c)

**Figure 5.2** Verification of capillary burst frequency carried out with blood  
(c) blood burst into reservoir C. (Continued)

The experiments with capillary burst valves have shown that due to their rpm-sensitive nature, the spinning time defines the flow rate in any particular channel. If the volume of liquid in the input reservoir is known then the flow rate could be estimated based on the time taken to empty the input reservoir completely. This observed flow rate ( $Q_o$ ) was compared to the theoretical flow rate ( $Q_T$ ) calculated using the following equation.

$$Q_T = \frac{1}{R} \Delta P$$

where,

$R$  = Fluidic resistance offered by the channel

$\Delta P$  = Difference in pressure at the two ends of the microchannel

For rectangular cross-sections the fluidic resistance is given by,

$$R = \frac{12\mu}{wh^3}$$

where,

w = width of the channel

h = height of the channel

$\mu$  = viscosity of the liquid

Therefore, the theoretical flow rate is given by,

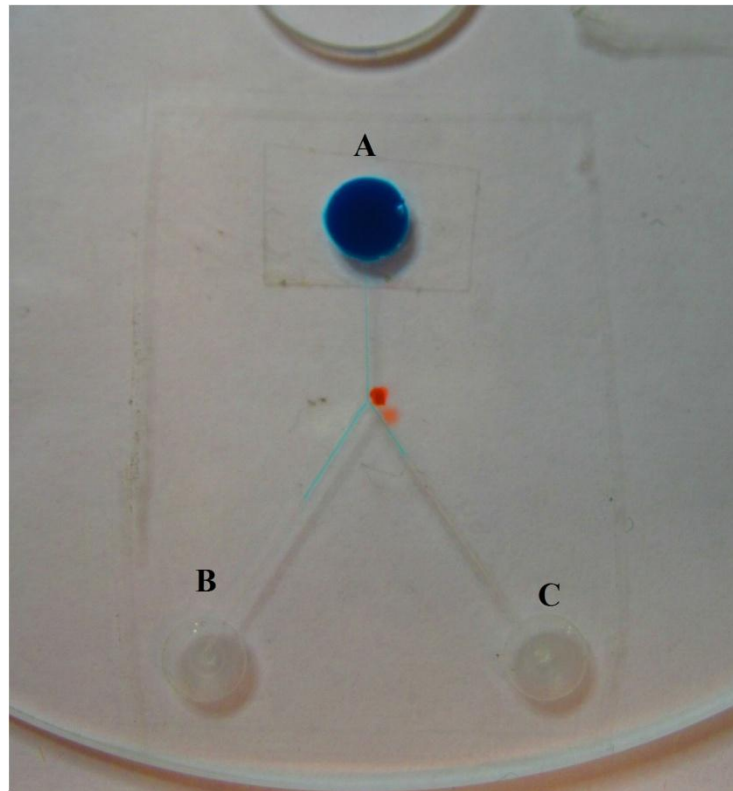
$$Q_T = \frac{wh^3\Delta P}{12\mu L} \quad - (5.1)$$

The observed flow rate was calculated by simply dividing the input volume by the time taken in seconds to completely empty the input reservoir. From the dimensions of the input reservoir the volume of the liquid contained was found to be 33 micro-litres. Time measurements were made with the help of a digital stopwatch. The time taken for the reservoir to empty out was measured after the fluid initially ‘burst’ from the capillary valve. This time was found to be 2.33 seconds at the burst frequency of 820 rpm mentioned in Table 5.1 for valve at B. The time taken to empty the reservoir B into reservoir C was measured to be 2.44 seconds. Thus, the experimental values for the flow rate from reservoir A to B was 11.67  $\mu\text{l/sec}$  and from reservoir B to C was found to be 10.89  $\mu\text{l/sec}$ .

The theoretical values were then calculated using equation 5.1. A channel cross-section of 200 X 170  $\mu\text{m}$  was considered for the calculations. The length of the channel from reservoir A to B was 0.85 cm and that from reservoir b to C was 0.9 cm. The viscosity of the water color was assumed to be  $1.002 \times 10^{-3} \text{ N s/m}^2$  since the room temperature ranged between 20 and 30 degrees Celsius. The theoretical values for the flow rate between reservoirs A and B was found to be 14  $\mu\text{l/sec}$  and that between B and C was found to be 13.36  $\mu\text{l/sec}$ . Therefore, good conformance between the theoretical and observed values for flow rates in the respective channels was seen.

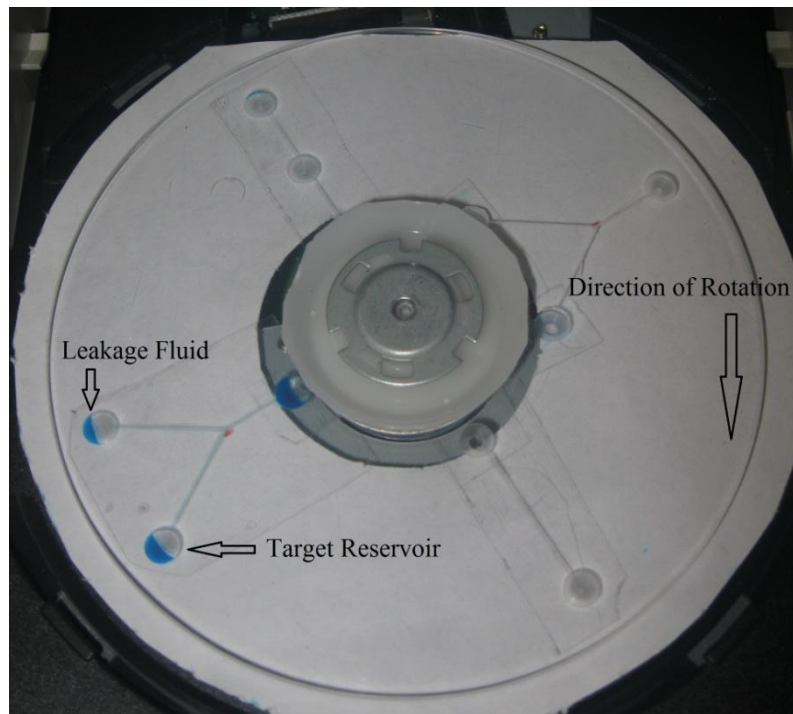
## 5.2 Coriolis-based Switching of Flow

As discussed in section 4.2, Coriolis force has been used to switch fluid flow into one of two outlets depending on the direction and speed of rotation. If the direction of rotation is changed then the fluid flow also switches its direction of flow. Further analysis of the rpm versus flow-switching efficiency was also performed to find the lowest frequency at which all of the liquid was directed to the target reservoir and no leakage was observed. Figure 5.3 shows the images from the experiment to find out the frequency at which no leakage occurs.

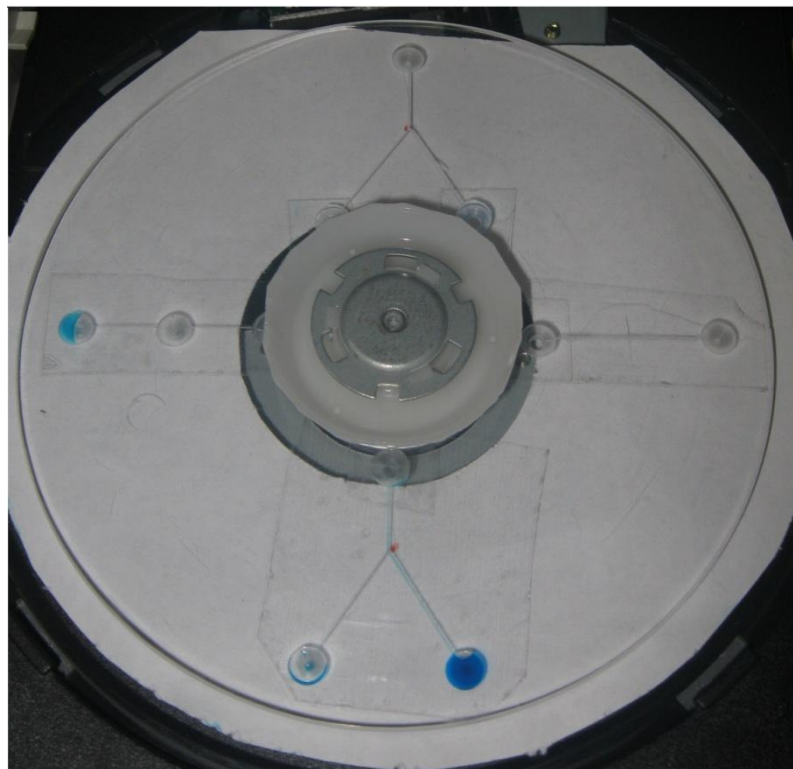


(a)

**Figure 5.3** Experiment to find the zero leakage rpm, (a) Input reservoir filled with water color initially.



(b)



(c)

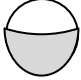
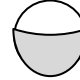
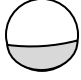

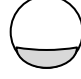
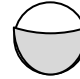


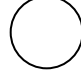
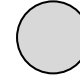
**Figure 5.3** Experiment to find the zero leakage rpm, (b) Leakage occurring at 630 rpm, (c) No leakage at 1050 rpm. (Continued)

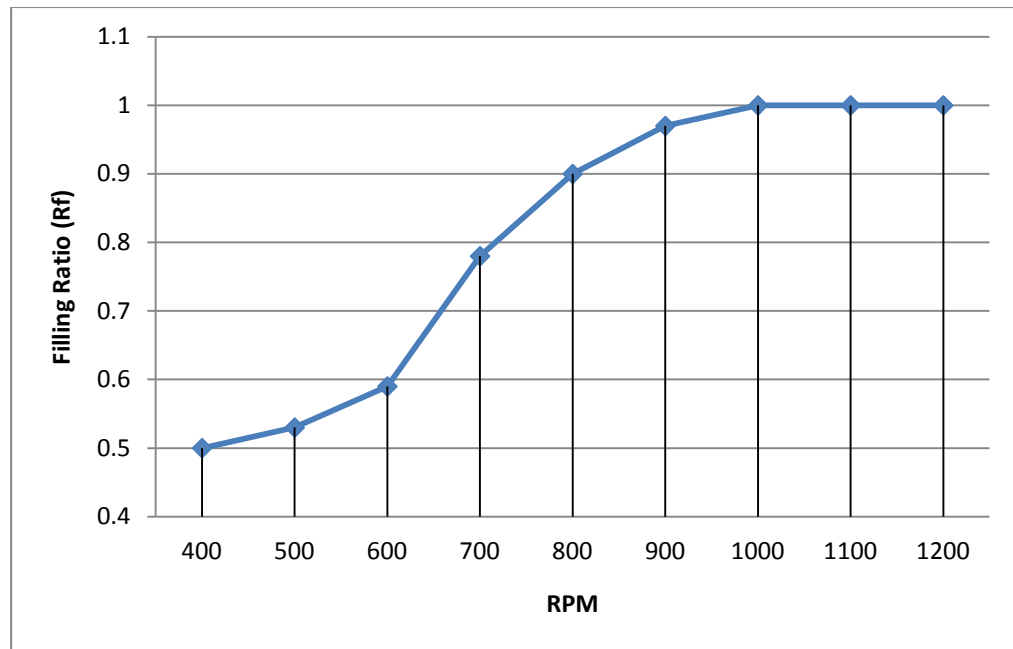
The input reservoir was loaded with the water color and the disk was spun. The rpm was increased in steps of 20 rpm starting from 500 rpm and the results were recorded at the end of every 15 seconds. Some sample points have been shown in Table 5.3. The height of liquid in both output reservoirs B and C was measured and recorded as  $h_B$  and  $h_C$ . A ratio of the height of the liquid in both reservoirs B and C was calculated as,

$$R_{c/b} = \frac{h_C}{(h_B + h_C)}$$

A graph of the values of this ratio has been plotted against the RPM of the disk to see the transition where the Coriolis force becomes more influential than the centrifugal force. The plotted graph showed good conformance with the graph reported in [19].

**Table 5.3** Results of the Coriolis-Based Flow Switch

	RPM	B	C	Ratio of liquid filling levels (R)
1	$500 \pm 20$			0.5
2	$620 \pm 20$			0.67
3	$750 \pm 20$			0.78
4	$880 \pm 20$			0.88
5	$1000 \pm 20$			1.0



**Figure 5.4** Graph of the filling ratio versus the rpm.

Theoretical values for the Coriolis and centrifugal forces were not calculated but the flow switching characteristics confirm that the results are in conformance with theory. Some of the errors in the measurements were caused due to the time taken to reach the desired rpm. The time delay in reaching the desired rpm causes fluid to leak into the reservoir B. The solution to this problem was to manually increase the rpm by turning the control potentiometer at runtime.

The Coriolis force was also used in conjunction with capillary burst valves to valve the flow of liquid as discussed in Section 4.2. The two geometries shown in Figure 4.7 were loaded with anti-coagulated blood simultaneously. The disk was then spun for 15 second intervals with rpm increments of 20 rpm per interval starting from 100 rpm. It was observed that the blood initially burst into the reservoir assisting the flow due to Coriolis force at 680 rpm whereas it burst into the reservoir opposing the Coriolis force at 760 rpm. Detailed theoretical analysis was not carried out but can be explored in the future. Figure 5.5 shows the images of the disk at 680 rpm and 760 rpm respectively to show the gating of blood.



(a)



(b)

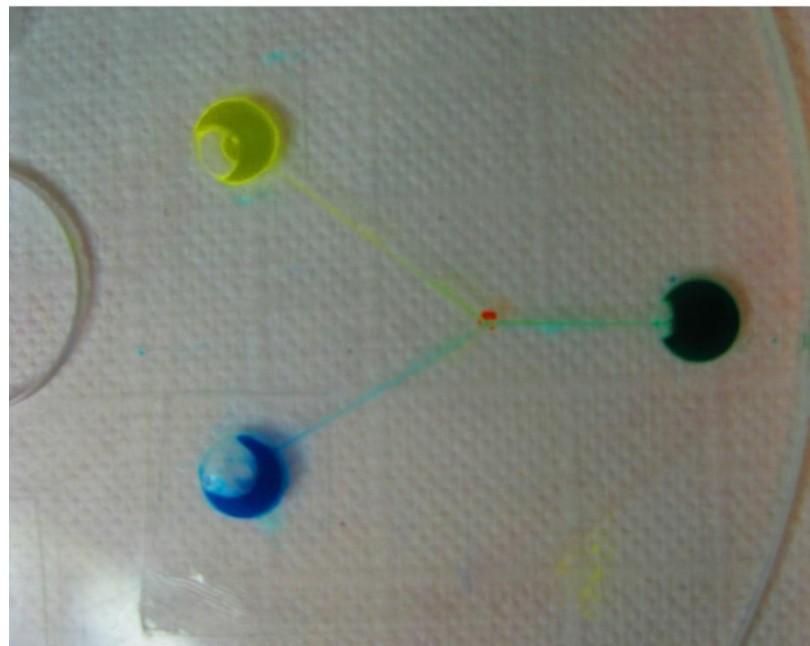
**Figure 5.5** Gating due to Coriolis force (a) Disk spinning at 680 rpm, (b) Disk spinning at 760 rpm.



### 5.3 Mixing of Two Fluids in Microchannels

The flow in microchannels is pre-dominantly a laminar flow (Renolds Number  $< 1000$ ). Therefore, the mixing of two liquids can only take place by diffusion between the two laminae of fluids inside the microchannel. As discussed in Section 4.3 the mixing of two fluids in centrifugal microfluidic channels was tested with the geometry shown in Figure 4.8. After spinning the disk at the rpm's mentioned in Section 4.3 mixing of the two fluids was observed as shown in Figure 5.6 (a).

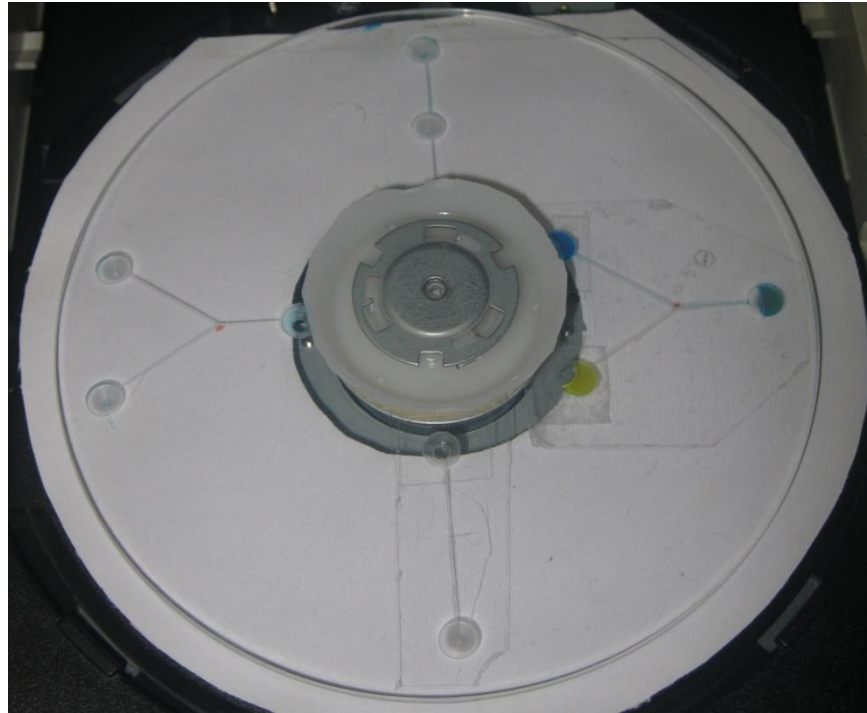
It was observed that the two water colors do mix and produce the green color after a while in the end reservoir. However, if the reservoir was observed while it was spinning then areas of different colored liquids are observed in the end reservoir as shown in Figure 5.6 (b).



(a)

**Figure 5.6** Mixing of two fluids in microchannels (a) after completion of spinning of the disk.





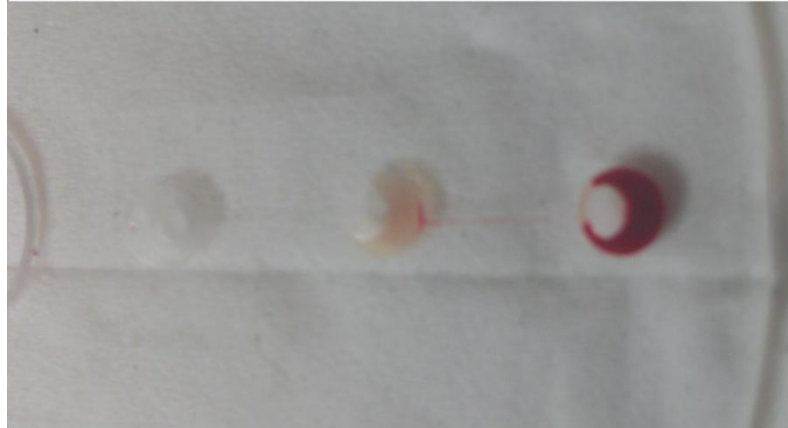
(b)

**Figure 5.6** Mixing of two fluids in microchannels (b) while the disk is still spinning. (Continued)

This suggests that diffusion in the end reservoir is the primary cause of mixing of the blue and yellow colors. Also, the bursting of the two fluids into the end reservoir may aid the mixing to some degree. The most popular technique for mixing fluids in microchannels is by using the multi-lamination of the flows to increase the diffusion surface area and reducing the diffusion length as discussed in [7].

#### 5.4 Separation of Plasma from Blood

Different geometries were tried for separating plasma from blood as discussed in Section 4.4. Initially, the simple geometry with capillary valves was used for plasma separation. The input reservoir was loaded with anti-coagulated blood and spun as described in section 4.4.1. Good separation of the blood plasma was observed at 1000 rpm as shown in Figure 5.7.



**Figure 5.7** Separation of plasma from blood using a geometry with just capillary valves.

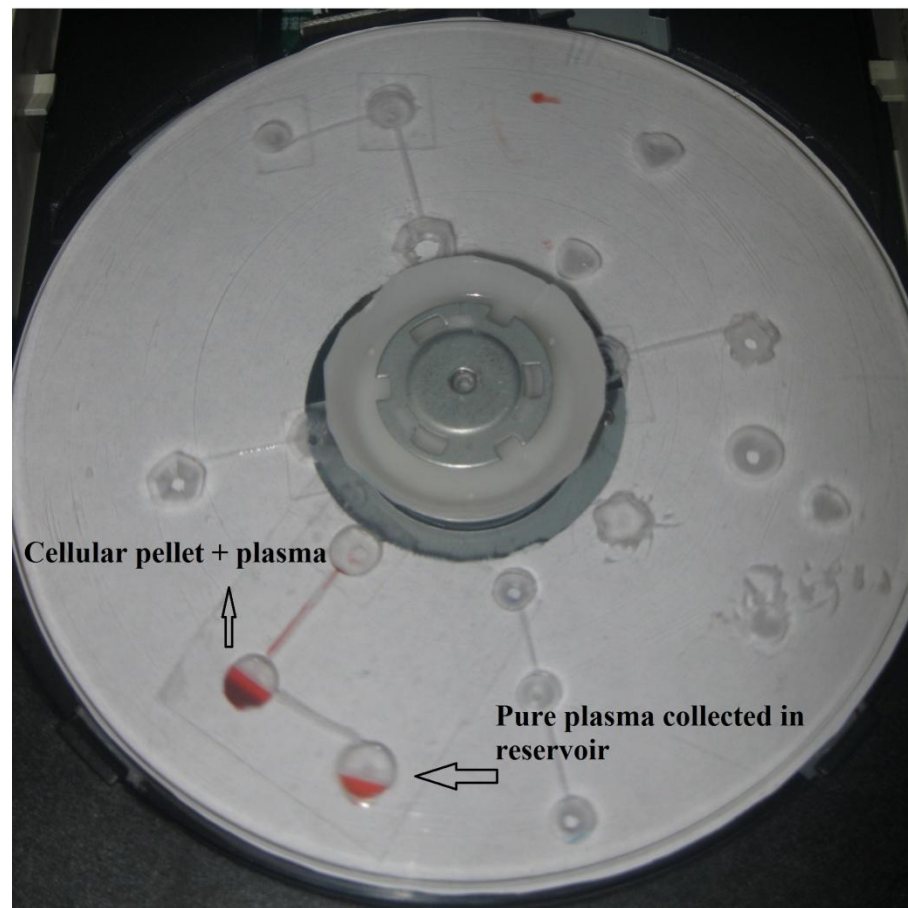
However, on multiple repetitions of this experiment it was found that this method of separating plasma from blood was highly time-dependent and therefore prone to error. Since the device did not have any timing control it would mean that manual intervention to stop the rotation of the disk at the precise moment would be required. This defeats the objective of having minimum or no manual intervention in the diagnostic procedure as discussed in Chapter 1. Hence, this geometry was not used for further experiments.

A micro-cyclone mechanism for separation of plasma from blood was implemented as discussed in Section 4.4.2. Different schemes for the inlet and outlet of the micro-cyclone were tried but the Coriolis Effect prevented the spiral flow of liquid inside the micro-cyclone. This led to poor separation and clogging was also observed in many cases. Figure 5.8 shows a sample geometry implementing the micro-cyclone being used for plasma separation. Although the micro-cyclone did not function well with the given dimensions, different combinations of dimensions and rotation frequencies could be experimented with in order to get better results.



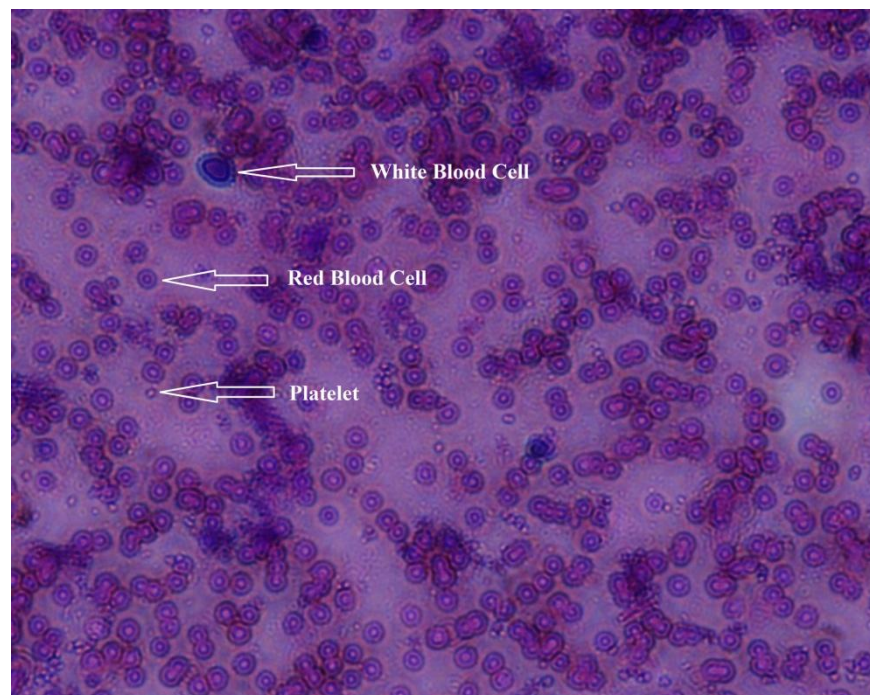
**Figure 5.8** Plasma separation using the micro-cyclone geometry.

The geometry discussed in Section 4.4.3 was the most successful in terms of separating plasma from blood. The experiment was performed as described in Section 4.4.3 and it was found that the plasma collected in reservoir 3 contained very few red-blood cells as shown in Figure 5.9. Since the separation efficiency was found to be high and the whole process was time-independent this method of plasma separation would be the best method to use for more complex analysis.



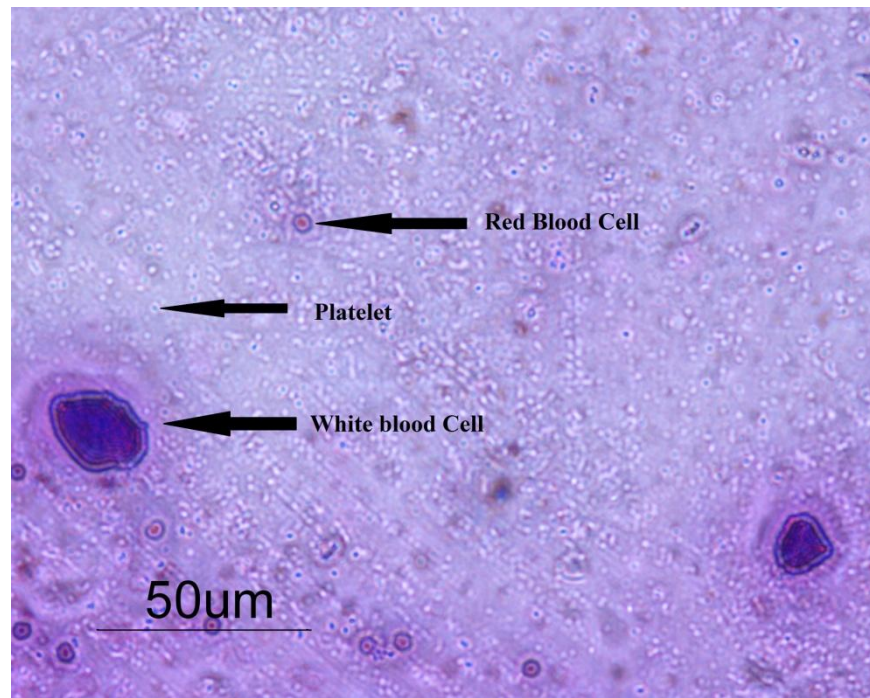
**Figure 5.9** Separation of plasma using the metering geometry.

The plasma collected in reservoir 3 seemed to be reddish in color if the blood was a couple of days old. This difference is clearly seen in Figure 5.7 and Figure 5.9. Hence, to look at the composition of the older plasma it was aspirated again in a syringe and tested for the presence of white blood cells. A drop of the collected plasma was put on a glass slide and was stained using the Wright's stain. Simultaneously a drop of whole blood was also put on a glass slide and stained in same way. Both the slides were observed under a microscope and color images were taken as shown in Figure 5.10. It was observed that the collected plasma (which was reddish in color) had some red blood cells suspended in it which gave it the red color. This leads to the conclusion that as the blood gets older the plasma proteins undergo some changes which prevent the red blood cells from separating out as efficiently as they would have done when the blood was fresh.



(a)

**Figure 5.10** (a) Whole blood imaged at 40X.



(b)

**Figure 5.10** (b) Separated plasma imaged at 40X. (Continued)

From the discussion about the composition of blood and erythrocytes in Section 2.1 it is known that percentage hematocrit can be directly used to detect disorders like Anaemia and Polycythemia. Thus, if the radial channel is placed at the normal hematocrit level by volume of the entity whose blood is being tested, conditions like Anaemia and Polycythemia can be diagnosed visually within minutes. If the plasma collection reservoir contains any red blood cells, then the patient can be said to have Polycythemia. Conversely, if the separation reservoir (reservoir 2) is seen to contain any plasma then the patient can be said to be Anaemic.



## **CHAPTER 6**

### **CONCLUSION AND FUTURE WORK**

#### **6.1 Conclusions**

The objective of this thesis was to demonstrate sample mixing, separation, flow control and detection using a centrifugal microfluidic device which is low-cost, reliable and portable. The prices of standalone CD-ROM drives have reduced greatly recently and therefore it lays the foundation for a great low-cost device. The electronic components used to control the rpm were also low-cost and easily available. Polycarbonate and acrylic disks have shown good results for basic centrifugal microfluidic applications. The rapid prototyping method used was fast, efficient and sufficiently accurate for creating the required geometries. The paper masks used to fabricate the geometry were easily produced. The channels were sealed with transparent Scotch tape which provided very good sealing of the whole geometry. The fabrication of the disks and conduction of experiments did not need a controlled environment, thus making it easy and less time consuming for performing the experiments. All of these attributes indicate that the device could be mass produced at low-cost thus reducing the overall cost-per-test.

The dimensions of the device without the power supply were 21cm × 15cm × 15cm. It weighed about 1 lb without the power supply and less than 2 lb with a compact power supply. The tray mechanism has shock absorbers to compensate for any vibrations that the motor may produce. Also, the CD-ROM drive is encased in a metal assembly which makes it very rugged.

This centrifugal platform proved that it can be used successfully to carry out experiments to verify the concepts of fluid dynamics without introducing too much

error in the expected results. The tasks of sample-reagent mixing, flow control, separation and detection required for more complex analysis were demonstrated successfully by the device. The range of rpm's provided by the CD-ROM was found to be suitable for working with blood as well as other fluids. Innovative geometries for handling fluid flows could be easily implemented and 100% pure plasma was separated efficiently from blood. Multiple repetitions of the same experiments yielded the same results with respect to burst frequencies, flow switching, mixing and separation. Hence, this device was found to be a reliable means for carrying out point-of-care testing.

The diagnostic procedures have been demonstrated to be completely driven by the laws of fluid mechanics and do not require tedious manual processing. This makes them reproducible and reliable. Also, as mentioned in the introduction the small sample sizes contribute to economy of operation and fast time-to-result of a diagnostic test. The ability to integrate multiple tests on a single disk also makes it an attractive medical product. The compact size of the device and the multi-functionality of the disks make it a portable device which can also be used in rural area without the supervision of a medical professional.

## **6.2 Future Work**

The device developed in this thesis was the first prototype of a centrifugal microfluidic platform developed in this lab. It provided sufficiently good control of the rpm of the compact disks for carrying out the preliminary experiments in gating/switching fluid flows and ultimately separating plasma from blood. However, the device could be improved more to become a marketable Point-Of-Care product. The following sub-sections elaborate on the possible improvements/upgrades that can

be made to the device to make it more user friendly, reliable, portable, economical and automated.

### **6.2.1 Instrumentation Upgrade**

Since the device was made out of an old computer CD-ROM drive it used the big bulky power supply of the Central Processing Unit (CPU). A compact power supply can be fabricated out of electronic components to supply the same voltages as the CPU power supply to make the device more compact and portable. Many external CD-ROM devices have an inbuilt compact power supply.

The rotation rpm was calculated from the output frequency of a square-wave signal generated by the 3-Phase Brushless DC Motor controller chip (TA 8493AF). A direct digital display of the instantaneous rpm can be designed using appropriate logic devices and seven-segment displays. During the course of the experiments it was found that the rpm would not stay completely stable in the given time interval which caused errors to occur in the readings. However, the focus of this thesis was on the biomedical possibilities of the application of this device and therefore the perfection of the controlling electronics and microchannel geometries was not carried out extensively. An electronic circuit can be easily designed to manipulate the control voltage  $V_c$  in the range of milli-volts or even micro-volts to give more accurate and stable control of the rpm. Finally, the time and rpm steps required in a particular diagnostic test could be pre-programmed on a micro-controller to give better automation to the user. Biological fluids have different viscosities and surface tensions which could be pre-configured in the software to give accurate estimates of the required rotation frequencies. Finally, a user-friendly graphical-user-interface (GUI) based screen could be developed to give the manufacturer the freedom to display a variety of languages thereby expanding the markets for the product globally.



Such data could then be transmitted from the remotely located patient site to a regional hospital for review and recommendation of treatment by panels of expert doctors in case of epidemics and other medical contingencies.

The optics of the CD ROM drive can be modified to perform Turbidometry amongst other imaging techniques for diagnostic applications. External imaging components can be added on and synchronized with the rotation of the disk to capture and display instantaneous images of strategic regions of the disk. Multiple tables of parameters could be stored on programmable memory built into the CD-OM device to set-up the intended operation in terms of rpm profiles and spinning times and b. comparison of the detected parameters with the sample 'healthy' values.

### **6.2.2 Microfabrication for Mass Production**

The compact disks used for making the geometries of microchannels were made of polycarbonate and acrylic. Both these materials have low bio-compatibility and are hydrophobic materials. Polydimethyl-siloxane (PDMS) is one of the many polymers which shows good bio-compatibility and is also easy to fabricate. The rapid prototyping method did not provide very accurate control of the geometries and channel dimensions which caused discrepancies in the results. Also, it was not possible to fabricate complex geometries using this method. CNC machining and/or laser printing can be used to produce high-aspect ratio micro-channels and complex geometries.

The Silicon industry has been using microfabrication technologies for mass production and proved them to be economical. A typical microfabrication procedure for making microchannels in PDMS is described in [5].

### **6.2.3 Advanced Biochemistry for Diagnosing Different Diseases**

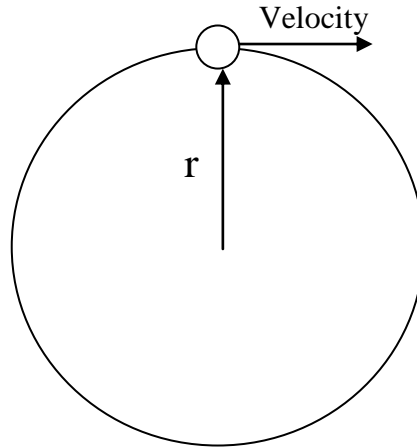
Recent advances in the field of biochemistry have brought forth interesting and useful diagnostic capabilities using biomarkers. Biomarkers are chemical or organic substances found in biological fluids which can be used to detect the presence or onset of an undiagnosed disease. Biomarkers have been discovered for detecting the presence of or the likelihood of developing leukemia, prostate cancer, etc. If the complex biochemistry diagnostic procedures can be translated onto the centrifugal microfluidic platform it would revolutionize the diagnostics industry.

Complex procedures like the Enzyme-linked Immunosorbent Assay (ELISA) have been successfully implemented in [10].

## APPENDIX A

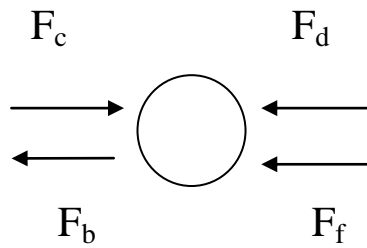
### ANALYSIS OF A PARTICLE ON A SPINNING DISC

The motion of a particle in the fluid well (i.e. a red blood cell) rotating on a disc can be described by the following:



**Figure A.1** Diagram of a particle on a spinning disc of radius  $r$ .

The free body diagram of a particle suspended in a fluid in the reservoir is shown below.



**Figure A.2** Free Body Diagram of a particle suspended in fluid in a reservoir.

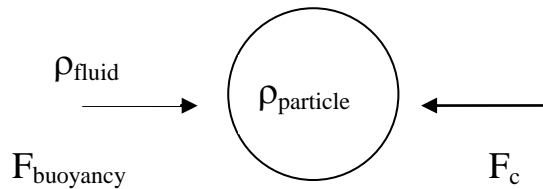
Where  $F_c$  is the centripetal force given by

$$F_c = m_p \frac{v^2}{r} = \rho_p V_p \omega^2 r$$

$\mathbf{F}_d$  is the drag force on the particle by the fluid as the particle moves through the fluid towards the wall. The heavy particles move towards the outside of the disk (closer to the wall) and the lighter particles move towards the center of the disk. As they move through the fluid there is a drag force on the particle given by

$$F_d = 6\pi r_p \mu v = 6\pi r_p \mu \omega r$$

$\mathbf{F}_b$  is the buoyancy force. A buoyancy force is due to the difference in densities between the particle and the fluid and acts in the direction opposite to the centripetal force (i.e. the normal force acting towards the center of the disc).

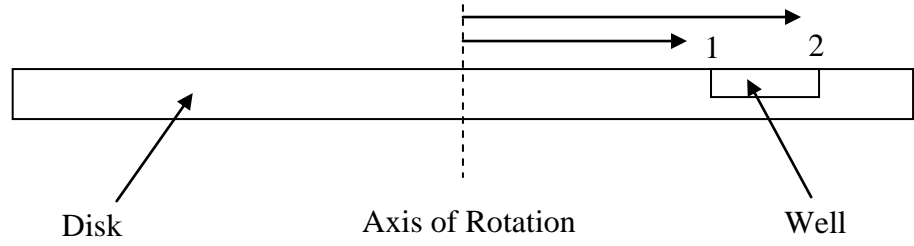


**Figure A.3** Explanation for the buoyancy force.

The mass of the fluid displaced by the particle is the density of the fluid times the volume of the particle.

$$F_b = ma = \rho_f V_p \omega^2 r$$

To find the fluid force on the particle,  $\mathbf{F}_f$ , we consider first the fluid pressure in the well.



**Figure A.4** Lateral view of a reservoir on a CD.

$$p_1 + \frac{1}{2}\rho_f\omega r_1 = p_2 + \frac{1}{2}\rho_f\omega r_2$$

$$\Delta p = \frac{1}{2}\rho_f\omega(r_2^2 - r_1^2)$$

$$\Delta p = \frac{1}{2}\rho_f\omega(r_2 - r_1)(r_2 + r_1)$$

Where  $r_2 - r_1 = D_{well}$  , the diameter of the well, and  $\frac{(r_2 + r_1)}{2} = r$  , the distance from center of the disc to the center of the well.

Therefore, the fluid pressure in the well is given by

$$\Delta p = \frac{1}{2}\rho_f\omega r D_{well}$$

Multiplying the pressure times the cross sectional area of the particle gives the force exerted by the fluid on the particle

$$F_f = \rho_f\omega^2 r D_{well} A_p$$

Where  $A_p$  is the cross sectional area of the particle given by  $\pi r_p^2$

Summing forces gives

$$F_c - F_d - F_b - F_f = m_p a_p$$

$$F_d + F_b + F_f = 0$$

After substituting we have

$$6\pi r_p \mu \omega r - \rho_f V_p \omega^2 r - \rho_f \omega^2 r D_{well} A_p = 0$$

And solving for omega gives the minimum frequency required to sort particles of a specified radius

$$\omega = \frac{-6\pi\mu r_p}{V_p \rho_f + \rho_f D_{well} \pi r_p^2}$$

Nomenclature:

$m_p$  = mass of particle

$a_p$  = acceleration on the particle

$\rho_p$  = particle density

$\rho_f$  = fluid density

$r_p$  = radius of particle

$V_p$  = Volume of particle  $V_p = \frac{4}{3}\pi r_p^3$

$r$  = radius from center of disc to center of fluid well

$D_{well}$  = Diameter of well

$\mu$  = fluid viscosity

**APPENDIX B**  
**DATASHEET – TA8493AF 3-PHASE BRUSHLESS DC MOTOR**  
**CONTROLLER**

Only the most relevant pages from the datasheet for the TA 8493AF have been included here. The other pages are out of the scope of the discussion of this thesis and have therefore been left out.

# TA8493F, TA8493AF, TA8493BF

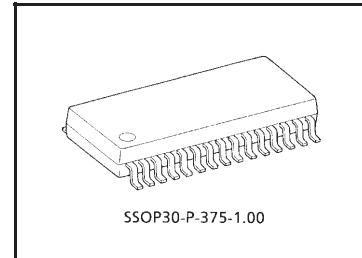
## 3-Phase Full Wave Brushless DC Motor Driver IC for CD-ROM Drives

These 3-phase, full-wave, brushless DC motor driver ICs have been developed for use in CD-ROM drive spindle motors. The TA8493F/AF/BF contain in its upper stage a discrete power transistor (P-ch-MOS) and uses direct PWM control system, which enables the IC to provide superior thermal efficiency.

Furthermore, the multi-chip structure of this device facilitates dispersion of the heat generated inside the package, making it possible to suppress heat concentration.

### Features

- Multi-chip structure ( $3 \times 2\text{SJ465}$  chips built-in)
- Direct PWM control system
- Drive system:  $120^\circ$  drive system (TA8493F/BF)  
:  $180^\circ$  drive system (TA8493AF)
- Built-in current limiter:  $I_{\text{LIM}} = 0.7 \text{ A}$  (typ.) (at  $R_F = 0.33 \Omega$ )
- Built-in reversing brake/short brake functions
- FG signal output (using hall element output signal)
- Built-in hall bias
- Built-in thermal shutdown circuit
- Package: MFP-30



Weight: 0.63 g (typ.)



**PIN Assignment**

Terminal No.	Terminal Symbol	Function	Remarks
1	L <sub>b</sub> (G)	b-phase upper side power transistor (base) output terminal	Keep open.
2	L <sub>a</sub> (G)	a-phase upper side power transistor (base) output terminal	Keep open.
3	L <sub>a</sub>	a-phase output terminal	Connect to the coil.
4	V <sub>M2</sub>	Supply voltage terminal for motor drive	Connect to V <sub>M1</sub> externally.
5	SB	RUN/STOP control terminal	H: RUN, L: STOP
6	R <sub>F1</sub>	Output current detection terminal	Sets limiter current value. Connect to R <sub>F2</sub> externally and between this terminal and GND.
7	GND2	GND	—
8	C <sub>RF</sub>	Output current filter terminal	Connect a capacitor between this terminal and GND.
9	N.C.		
10	FGO	FG amplifier output terminal	Outputs a signal whose frequency is determined by the CD rotation frequency.
11	BRK	Brake mode select terminal	Output mode when V <sub>C</sub> > V <sub>ref</sub>
12	H <sub>b</sub> <sup>-</sup>	b-phase negative hall signal input terminal	Connect to hall element output terminal.
13	H <sub>b</sub> <sup>+</sup>	b-phase positive hall signal input terminal	Connect to hall element output terminal.
14	H <sub>a</sub> <sup>-</sup>	a-phase negative hall signal input terminal	Connect to hall element output terminal.
15	H <sub>a</sub> <sup>+</sup>	a-phase positive hall signal input terminal	Connect to hall element output terminal.
16	H <sub>c</sub> <sup>+</sup>	c-phase positive hall signal input terminal	Connect to hall element output terminal.
17	H <sub>c</sub> <sup>-</sup>	a-phase negative hall signal input terminal	Connect to hall element output terminal.
18	HB	Hall element bias terminal	Open collector output. Connect to the negative side of hall element bias line.
19	C <sub>d</sub>	Forward/reverse changeover gain adjustment terminal	Adjust a rotation direction changeover gain
20	V <sub>CC</sub>	Supply voltage terminal for control circuits	V <sub>CC (opr)</sub> = 4.5 to 5.5 V
21	V <sub>C</sub>	Control amplifier input terminal	Use the control signal as input.
22	V <sub>ref</sub>	Control amplifier reference voltage input terminal	Use the reference voltage for the control amplifier as input.
23	OSC	Triangular wave oscillation terminal	Connect a capacitor between this terminal and GND.
24	GND1	GND	—
25	R <sub>F2</sub>	Output current detection terminal	Sets limiter current value. Connect to R <sub>F1</sub> externally and between this terminal and GND.
26	MS	Mode select terminal	Determines output mode.
27	L <sub>c</sub> (G)	c-phase upper side power transistor (base) output terminal	Keep open.
28	L <sub>c</sub>	c-phase output terminal	Connect to the coil.
29	V <sub>M1</sub>	Supply voltage terminal for motor drive	Connect to V <sub>M2</sub> externally.
30	L <sub>b</sub>	b-phase output terminal	Connect to the coil.

**Absolute Maximum Ratings (Ta = 25°C)**

Characteristics	Symbol	Rating	Unit
Power Supply Voltage	V <sub>CC</sub>	7	V
	V <sub>M</sub>	16	
Output Current	I <sub>O</sub>	1.5	A
Power Dissipation	P <sub>D</sub> (Note1)	1.0	W
Junction Temperature	T <sub>j</sub>	150	°C
Operating Temperature	T <sub>opr</sub>	-20 to 75	°C
Storage Temperature	T <sub>stg</sub>	-55 to 150	°C

Note1: unmounted

**Operating Voltage Range**

Characteristics	Symbol	Operating Range	Unit
Power Supply Voltage	V <sub>CC</sub>	4.5 to 5.5	V
	V <sub>M</sub>	10 to 14	

**Electrical Characteristics (V<sub>CC</sub> = 5 V, V<sub>M</sub> = 12 V, Ta = 25°C)**

Characteristics		Symbol	Test Circuit	Test Condition	Min	Typ.	Max	Unit
Supply Voltage		I <sub>CC1</sub>	1	Stop mode	—	0.3	0.8	mA
		I <sub>CC2</sub>		Run mode, output open	—	7	15	
Hall Amp.	Input Current	I <sub>INH</sub>	2	V <sub>CMRH</sub> = 2.5 V, (sink current)	—	—	2	μA
	Common Mode Input Voltage Range	V <sub>CMRH</sub>		—	1.5	—	4.0	V
	Input Amplitude	V <sub>H</sub>		—	100	—	—	mV <sub>p-p</sub>
Hall Element Bias Saturation Voltage		V <sub>HB</sub>	2	I <sub>HB</sub> = 10 mA	—	1.3	2.0	V
Control Amp.	Common Mode Input Voltage Range	V <sub>CMRC</sub>	2	—	0.5	—	4.0	V
	Input Current	I <sub>INC</sub>		V <sub>C</sub> = V <sub>ref</sub> = 1.65 V, (source current)	—	—	5.0	μA
	Dead Zone Voltage Width	V <sub>DZ</sub>	—	V <sub>ref</sub> = 1.65 V, R <sub>F</sub> = 0.33 Ω (Note2)	—	100	—	mV
	Input Offset Voltage	ΔV <sub>OFF</sub> (F)	2	CW mode, V <sub>ref</sub> = 1.65 V, R <sub>F</sub> = 0.33 Ω	20	50	150	
		ΔV <sub>OFF</sub> (R)		CCW mode, V <sub>ref</sub> = 1.65 V, R <sub>F</sub> = 0.33 Ω	20	50	150	
Current Limit Amp.	Limit Current	I <sub>LIM</sub>	—	R <sub>F</sub> = 0.33 Ω (Note2)	—	700	—	mA
		V <sub>LIM</sub>	3	—	0.25	0.3	0.35	V
RUN/STOP Control Circuit	Input Voltage (H)	V <sub>INS</sub> (H)	1	(RUN)	3.0	—	V <sub>CC</sub>	V
	Input Voltage (L)	V <sub>INS</sub> (L)		(STOP)	GND	—	1.0	
	Input Current	I <sub>INS</sub> (L)		V <sub>INS</sub> = GND, (source current)	—	—	1	μA

Note2: this is not tested.

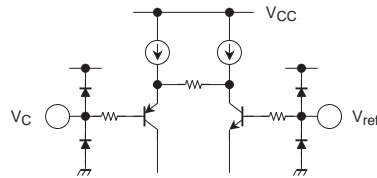
Characteristics		Symbol	Test Circuit	Test Condition	Min	Typ.	Max	Unit
Output Circuit	Output Resistance (upper side)	$R_{ON} (U)$	4	$I_O = 0.6 \text{ A}$	—	0.5	1.0	$\Omega$
	Saturation Voltage (lower side)	$V_{SAT} (L)$		$I_O = 0.6 \text{ A}$	—	0.4	0.8	V
	Cut-off Current (upper side)	$I_L (U)$	5	$V_L = 16 \text{ V}$	—	—	10	$\mu\text{A}$
	Cut-off Current (lower side)	$I_L (L)$		$V_L = 16 \text{ V}$	—	—	10	
Mode Select Circuit	Input Voltage (H)	$V_{MS} (H)$	6	CCW mode $V_C > V_{ref}$ , BRK: L	3.0	—	$V_{CC}$	V
	Input Voltage (L)	$V_{MS} (L)$		Reversing brake mode $V_C > V_{ref}$ , BRK: L	—	—	0.5	
	Input Current	$I_{INMS}$		$V_{MS} = \text{GND}$ , (source current)	—	—	1	$\mu\text{A}$
FG Amp.	Hysteresis Voltage	$V_{HYS}$	8	—	5	20	45	mV <sub>p-p</sub>
	Output Voltage (H)	$V_{OFG} (H)$	7	Source current: 10 $\mu\text{A}$	$V_{CC} - 0.5$	—	—	V
	Output Voltage (L)	$V_{OFG} (L)$		Sink current: 10 $\mu\text{A}$	—	—	0.5	
Short Brake Circuit	Input Voltage (H)	$V_{BRK} (H)$	6	—	3.0	—	$V_{CC}$	V
	Input Voltage (L)	$V_{BRK} (L)$		—	—	—	0.5	
	Input Current	$I_{INBRK}$		$V_{BRK} = \text{GND}$ , (source current)	—	—	1	$\mu\text{A}$
Triangular Oscillation Circuit	Oscillation Frequency	$f_{OSC}$	—	$C = 560 \text{ pF}$ (Note2)	—	39	—	kHz
Thermal Shut-down Operating Temperature		TSD	—	Junction temperature (according to design specification) (Note2)	—	175	—	$^{\circ}\text{C}$

Note2: this is not tested.

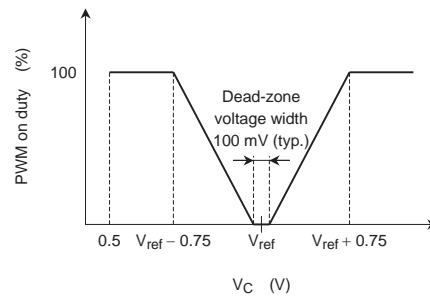
### Functional Description

This IC is a 3-phase, full wave brushless DC motor driver of the direct PWM control type.

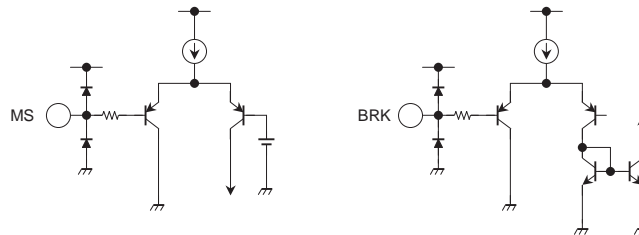
- Control amp input circuit



The common mode input voltage ranges for both  $V_C$  and  $V_{ref}$  are 0.5 to 4.0 V.  
 Relation between control input and PWM ON duty is shown below, PWM ON duty is 100% when  $|V_{ref} - V_C| = 0.75$  V (typ.)  
 The input is provided with a dead-zone area whose voltage width is 100 mV (typ.)



- Mode select/short brake circuit



When  $V_C > V_{ref}$ , one of three modes (reverse rotation, reversing brake or short brake mode) can be selected by setting the MS and BRK pins appropriately.

<Function>

$V_C < V_{ref}$

		BRK	
		H	L
MS	H	Forward	Forward
	L	Forward	Forward

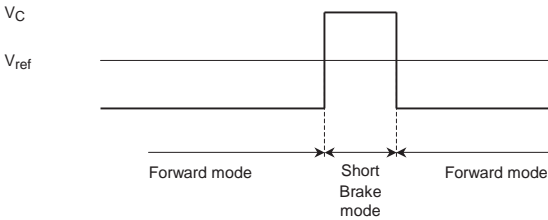
$V_C > V_{ref}$

		BRK	
		H	L
MS	H	Short brake	Reverse
	L	Short brake	Reversing brake

In Short Brake mode, the upper-stage power transistor is turned on and the lower-stage power transistor is turned off.

(short brake)

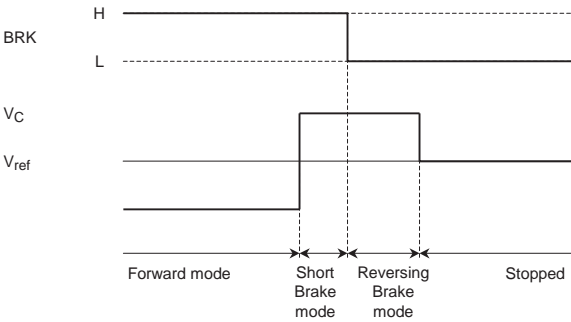
MS: H or L, BRK: H



(reversing brake)

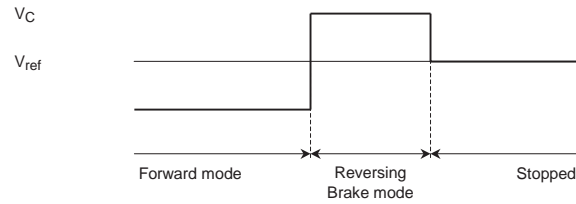
(1) When stopping the motor by applying a reversing brake after a short brake

MS: L



- (2) When stopping the motor using reversing brake mode

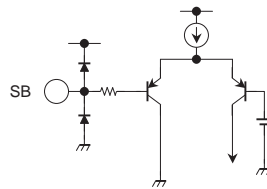
MS: L, BRK: L



Note3: For an explanation of the Reversing Brake mode stopping sequence, refer to the explanation of the reverse rotation detection circuit.

The short brake generates less heat than the reversing brake. Therefore Toshiba recommends a combined use of the short and reversing brakes when stopping the motor.

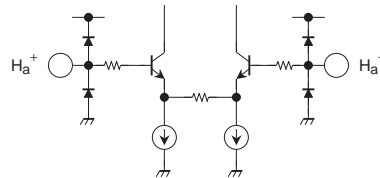
- Run/stop control circuit



When the driver IC is standing by, all of its circuits except the FG amp and the hall amp are turned off.

H: start  
L: standby

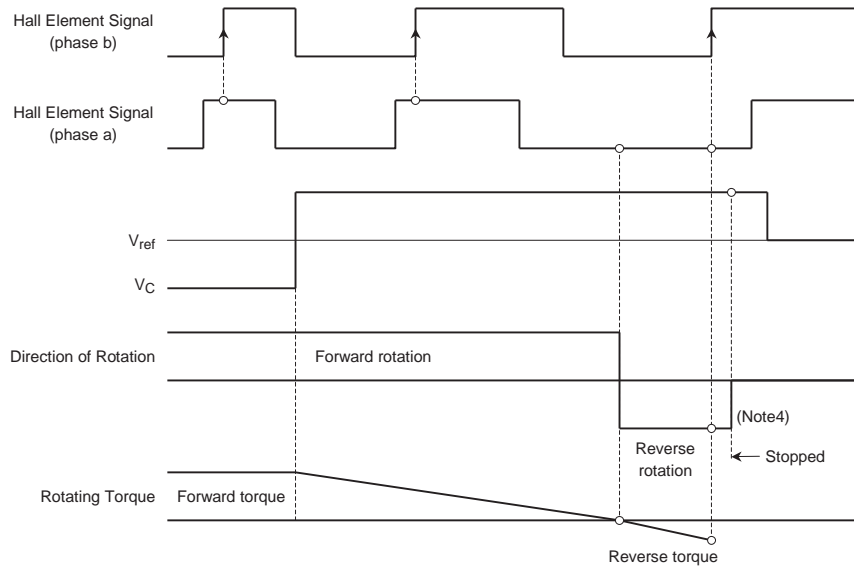
- Hall amp circuit



The common mode input voltage range for VCMRH is 1.5 to 4.0 V.

- Reverse rotation detection circuit

By comparing the two phases of the Hall element signal, this circuit detects a state where the phases are inverted, at which time the torque is reduced to 0. The detection accuracy is determined by the number of pulses per rotation of Hall element output.



Note4: Due to its inertial force, the motor does not stop immediately after the torque is reduced to 0.

## REFERENCES

- [1] Zoval, J.V. and M.J. Madou, "Centrifuge-based fluidic platforms". *Proceedings of the IEEE*, 2004. 92(1): p. 140-153.
- [2] Gorkin, R. and et al., "Centrifugal microfluidics for biomedical applications". *Lab on a Chip*, 2010. 10(14): p. 1758.
- [3] Halpern, N.A., "Point Of Care Diagnostics and Networks". *Critical Care Clinics*, 2000. 16(4): p. 623-39.
- [4] Madou, M.J., et al., "Design and fabrication of CD-like microfluidic platforms for diagnostic: Microfluidic functions". *Biomedical Microdevices*, 2001. 3(3): p. 245-254.
- [5] Lee, L.J., et al., "Design and fabrication of CD-like microfluidic platforms for diagnostics: Polymer-based microfabrication". *Biomedical Microdevices*, 2001. 3(4): p. 339-351.
- [6] Todd M. Squires, S.R.Q., "Microfluidics: Fluid Physics at the nano-liter scale". *REVIEWS OF MODERN PHYSICS*, 2005. 77.
- [7] Jens Ducree, e.a., "Multilamination of flows in planar networks of rotating microchannels". *Microfluid Nanofluid*, 2005. 2(1): p. 78-84.
- [8] Siyi Lai, et al., "Design of a Compact Disk-like Microfluidic Platform for Enzyme-Linked Immunosorbent Assay". *Analytical Chemistry*, 2004. 76(7): p. 1832-1837.
- [9] Jens Ducree, T.B., Thomas Glatzel and Roland Zengerle, "Coriolis-effects-mixing in rotating microchannels".
- [10] Yusoff, N.A., N. Soin, and F. Ibrahim. Lab-on-a-disk as a potential microfluidic platform for dengue NS1-ELISA. in *Industrial Electronics & Applications, 2009. ISIEA 2009. IEEE Symposium on*. 2009.
- [11] Focke, M., et al., "Centrifugal microfluidic system for primary amplification and secondary real-time PCR". *Lab on a Chip*, 2010. 10(23): p. 3210.
- [12] Garcia-Cordero, J.L., et al., "Liquid recirculation in microfluidic channels by the interplay of capillary and centrifugal forces". *Microfluidics and Nanofluidics*, 2010.
- [13] Steigert, J., et al., "Direct hemoglobin measurement on a centrifugal microfluidic platform for point-of-care diagnostics". *Sensors and Actuators A: Physical*, 2006. 130-131: p. 228-233.
- [14] Steigert J., et al., "Fully integrated whole blood testing by real-time absorption measurement on a centrifugal platform". *Lab on a Chip*, 2006. 6(8): p. 1040



- [15] David C. Duffy, et al., "Microfabricated Centrifugal Microfluidic Systems: Characterization and Multiple Enzymatic Assays". *Analytical Chemistry*, 1999. 71(20): p. 4669-4678.
- [16] Gorkin Iii, R., et al., "Pneumatic pumping in centrifugal microfluidic platforms". *Microfluidics and Nanofluidics*, 2010(Journal Article): p. 1-9.
- [17] Mir, M., et al., "Diffraction phase cytometry: Blood on a CD-ROM". *Optics Express*, 2009. 17(4): p. 2579-2585.
- [18] Sung-Woo, L., et al. Single cell assay on cd-like lab chip using centrifugal single cell trap. in *Micro Electro Mechanical Systems, 2007. MEMS. IEEE 20th International Conference on*. 2007.
- [19] Jitae Kim, et al., "Passive flow switching valves on a centrifugal microfluidic platform". *Sensors and Actuators*, 2007. B(128): p. 613- 621.
- [20] Sung Yang, Akif Undar, and J.D. Zahn, "A microfluidic device for continuous, real-time blood plasma separation". *Lab on a Chip*, 2006. 6: p. 871-880.
- [21] J. L. Garcia-Cordero, I.K.D., J. Ducree "Monolithic Centrifugal Microfluidic Platform for bacteria capture and concentration,. lysis, nucleic-acid amplification and real-time detection". *IEEE*, 2009: p. 356-359.
- [22] Leu, T.S. and P.Y. Chang, "Pressure barrier of capillary stop valves in micro sample separators". *Sensors and Actuators, A: Physical*, 2004. 115(2-3 SPEC. ISS.): p. 508-515.
- [23] Yoon-Kyoung, C., et al. One-Step Pathogen Specific DNA Extraction from Whole Blood on a Centrifugal Microfluidic Device. in *Solid-State Sensors, Actuators and Microsystems Conference, 2007. TRANSDUCERS 2007. International*. 2007.
- [24] Siegrist, J., et al., "Serial siphon valving for centrifugal microfluidic platforms". *Microfluidics and Nanofluidics*, 2009.
- [25] LaCroix-Fralish, A., et al., "A rapid prototyping technique for valves and filters in centrifugal microfluidic devices". *Lab on a Chip*, 2009. 9(21): p. 3151.
- [26] Hansang Cho\*, H.-Y.K., Ji Yoon Kang\*, and Tae Song Kim\*, "Capillary passive valve in microfluidic systems". *NSTI-Nanotech 2004*, 2004. 1: p. 263-266.
- [27] Jun Zeng, D.B., Manish Deshpande and John R. Gilbert, "Design analysis of capillary burst valves in centrifugal microfluidics".
- [28] Anton A. Darhuber, J.P.V., Sandra M. Troian, and SigurdWagner, "Thermocapillary Actuation of Droplets on Chemically Patterned Surfaces by Programmable Microheater Arrays". *JOURNAL OF MICROELECTROMECHANICAL SYSTEMS*, 2003. 12(6): p. 873-879.
- [29] Reigger, L., "Single-step centrifugal hematocrit determination on a 10-\$ processing device". *Biomed Microdevices*, 2007.
- [30] Park, J.M., et al. One-step white blood cell separation from whole blood on a centrifugal microfluidic device. in *2008 NSTI Nanotechnology Conference and Trade Show, NSTI Nanotech 2008 Joint Meeting, Nanotechnology 2008*.

- [31] Steigert, J., et al., "Integrated Sample Preparation, Reaction, and Detection on a High-frequency Centrifugal Microfluidic Platform". 2005. 10(5): p. 331-341.
- [32] Steigert, J., et al., "Integrated siphon-based metering and sedimentation of whole blood on a hydrophilic lab-on-a-disk". *Biomedical Microdevices*, 2007. 9(5): p. 675-679.
- [33] Steigert, J., et al. Design and Fabrication of a Centrifugally Driven Microfluidic Disk for Fully Integrated Metabolic Assays on Whole Blood. in *Micro Electro Mechanical Systems, 2006. MEMS 2006 Istanbul. 19th IEEE International Conference on*. 2006.
- [34] Ezekiel Uba Nwose, P., CSci, FIBMS, MAIMS., "Whole blood viscosity assessment issues: Extrapolation chart and reference values". *North American Journal of Medical Sciences*, 2010. 2(4): p. 165-169.
- [35] Lee Waite and J. Fine, Applied Biofluid Mechanics, in *Applied Biofluid Mechanics*. 1999.
- [36] Barbee, J.H.a.G.R.C., "The Fahreus Effect". *Microvasc Res*, 1971. 3: p. 6-16.
- [37] D. Trebotich, W. Chang, and D. Liepmann, "Modelling of Blood Flow in Simple Microchannels", in *Modelling and Simulation of Microsystems*. 2001, IEEE: France.